Mathematical modeling unveils the timeline of CAR-T cell therapy and macrophage-mediated cytokine release syndrome

Daniela S. Santurio[1], Luciana R. C. Barros[2], Ingmar Glauche[3], Artur C. Fassoni[3,4,*]

[1]Certara UK Ltd., Sheffield, United Kingdom
[2]Instituto do Câncer do Estado de São Paulo, São Paulo, Brazil
[3]Institute for Medical Informatics and Biometry, Technische Universität Dresden, Dresden, Germany
[4]Instituto de Matemática e Computação, Universidade Federal de Itajubá, Itajubá, Brazil
[*]corresponding author: fassoni@unifei.edu.br

Abstract

Chimeric antigen receptor (CAR)-T cell therapy holds significant potential for cancer treatment, although disease recurrence and cytokine release syndrome (CRS) remain as frequent clinical challenges. To better understand the underlying mechanisms and temporal dynamics during CAR-T cell therapy response we developed a novel multi-layer mathematical model that accurately describes 25 patient time-courses with diverse responses and IL-6 cytokine kinetics. We successfully link the dynamic shape of the response to interpretable model parameters and study the influence of CAR-T cell dose and initial tumor burden on CRS occurrence and treatment outcome. Further accounting for three established mechanisms of macrophage activation we identified the CD40-CD40L axis as a clinically feasible target to control the activation process and modulate IL-6 peak height. Our study underscores the utility of mechanistic modeling in deciphering therapy dynamics and guiding clinical interventions, emphasizing the importance of close integration with clinical data.

Introduction

Immunotherapy with chimeric antigen receptor T (CAR-T) cells is a groundbreaking approach that harnesses the power of the immune system to fight hematological and non-hematological malignancies [1]. Genetic engineering enables T cells to express chimeric antigen receptors (CARs), enhancing their ability to specifically recognize and eliminate cancer cells. This remarkable efficacy in treating certain types of blood cancers made CAR-T cell therapy a promising avenue in oncology, with new CAR designs entering clinical trials for several indications, including solid tumors [2].

The short-term response to CAR-T cell therapy is characterized by typical multiphasic dynamics, with the initial distribution phase being marked by a decline of injected cells due to their death and migration to tumor site. The subsequent expansion phase encompasses tumor-killing and a massive proliferation of CAR-T cells mediated by antigen recognition. In the following contraction phase, exhausted CAR-T cells are eliminated, and a fraction of long-lived memory CAR-T cells remain in the final persistence phase. Using mathematical models we and others showed how this multiphasic dynamics emerge from the interaction of different CAR-T cell phenotypes with tumor cells [3, 4, 5].

While CAR-T cell therapy is as a paradigm-shifting modality for cancer treatment, it faces substantial challenges, with 30-60% of patients experiencing recurrence within one year post-treatment [6]. Its effectiveness is linked to biological mechanisms of CAR-T cells, such as expansion, cytotoxicity, and memory formation, all of which are influenced by antigen recognition. Consequently, the density of antigens presented by tumor cells constitutes a pivotal factor for therapy resistance. Modeling this density as a continuous variable, we showed that transient antigen loss under treatment pressure or permanent antigen loss due to mutations account for typical resistance mechanisms [7]. However, due to the specific data needed for calibration (namely time courses of tumor antigen density), this model is primarily suited for theoretical insights and requires simplification for application in a clinical context.

Besides resistance, major obstacles for CAR-T cell therapy are side effects, including cytokine release syndrome (CRS) and immune effector cell-associated neurotoxicity syndrome (ICANS) [8]. Affecting 13%-26% of patients, severe CRS is the most prevalent adverse event[9], with symptoms typically emerging 1-7 days post-infusion [10], commonly before the CAR-T cell peak [9]. CRS is characterized by fever, hypotension, and respiratory insufficiency and is associated with rising levels of cytokines, including IL-6, IL-10, IL-8, interferon-γ (IFN-γ) and granulocyte–macrophage colony-stimulating factor (GM-CSF) [11, 12]. In many cases CRS severity is tied to tumor burden and sometimes to CAR-T cell dose [13]. CRS also influences patient survival, and severe CRS (grade 3-5) correlated with lower survival in multiple myeloma (MM) and acute lymphoid leukemia (ALL) patients [11, 12].

Preclinical studies suggest that CRS results from complex interactions between CAR-T and host cells, with macrophages as a primary source of released cytokines [14, 15, 16, 8]. Three mechanisms have been identified as major drivers of macrophage activation underlying CRS [8]. First, upon antigen-binding-mediated activation, CAR-T cells release inflammatory signals such as IFN-γ and GM-CSF that induce macrophage activation in a contact-independent manner. Second, following tumor cell targeting by CAR-T cells, damage-associated molecular patterns (DAMPs) released by pyroptotic tumor cells enhance macrophage activation through pattern-recognition receptors. Third, the interaction of CD40 expressed on activated macrophages with CD40L expressed on CAR-T cells further promotes macrophage activation in a contact-dependent manner.

Different aspects of CAR-T cell therapy were investigated by modeling approaches [17, 18, 19, 20] with a few focusing on CRS [21, 22, 23, 24]. However, the critical role of macrophages on cytokine release was rarely addressed [25]. It is currently unclear how the different macrophage-associated mechanisms influences the extent and the temporal dynamics of CRS, although these aspects are essential for clinical implementation of countermeasures. With refined models, therapeutic interventions can be tested, as for example modulating CAR-T cell dose or changes in preconditioning to reduce the initial tumor burden. The models can also describe supportive administration of different corticosteroids

or antibodies to inhibit macrophage activation and cytokine release.

Here, we develop a novel, multi-layer model of CAR-T cell therapy encompassing antigen-negative resistance and macrophage-associated cytokine release. The model consistently describes time courses of 25 patients with different malignancies and tumor responses. Explicitly including three mechanisms of macrophage activation (DAMPs release, antigen-binding, and CD40 contact), the model also fits to cytokine time courses of 15 patients. We dissect the different phases of macrophage activation, showing that each mechanism occurs at a different time point during therapy response, with different contributions. Our results provide insights on macrophage-mediated cytokine release and elicit testable hypotheses on therapeutic interventions to mitigate CRS in CAR-T cell therapy.

Results

The model accurately reproduces diverse patient-specific responses

The fundamental layer of our modeling approach is a minimal mechanistic model describing CAR-T cell multiphasic dynamics and antigen-positive tumor responses (Fig. 1a, equations (1-5)). This layer encompasses three CAR-T cell phenotypes, namely injected, effector, and memory cells, and a population of antigen-positive tumor cells. The underlying model emerges as simplification from our previous model [5] with a reduction from 19 to 12 parameters, now integrating concepts of T-cell turnover [26] which explain transitions between CAR-T cell phenotypes as functional responses to antigen-binding (Fig. 1a). In short, the antigen load activates injected CAR-T cells, triggers the expansion of effector CAR-T cells, and converts memory cells into effector cells while inhibiting memory formation from effector cells. Fitting the model to time courses of n=19 CAR-T-treated patients with different malignancies (Fig. 2, Supplementary Figs. 1 and 2), shows that the model accurately describes both the CAR-T cell multiphasic dynamics as well as the different types of tumor responses.

Tumor relapse occurs in 30-60% of patients within one year after CAR-T therapy [6] and many relapsed patients present antigen-negative tumor cells, which are more resistant to CAR-T cytotoxicity. To account for those cases, we add a second layer to the basic model, consisting of a population of antigen-negative tumor cells (Fig. 1b, equation (7)). Due to the lack of antigen, we assume that these cells do not contribute to the antigen-mediated phenotypic changes in CAR-T cells. However, they are subject to a minimal cytotoxic effect by CAR-T cells due to the bystander effect and CAR-T cell endogenous T-cell receptor [28, 7]. The model was fitted to $n = 6$ time courses of antigen-negative relapsed patients (Fig. 2, Supplementary Fig. 3). We confirm that the model quantitatively and qualitatively reflects the dynamics of antigen-negative relapses.

To detect early indications of severe CRS in CAR-T cell therapy, the concentrations of critical cytokines are usually monitored in parallel to treatment response, specifically IL-6. Typically, these cytokines follow a predictable kinetics: starting from a baseline concentration, they often peak before the CAR-T cell peak, and then return to baseline levels. It is increasingly evident that macrophages play a pivotal role in the release of cytokines in response to CAR-T cell therapy [14, 16, 8]. To quantitatively describe macrophage-mediated cytokine kinetics and gain a deeper understanding on the mechanisms underlying CRS, we add a third layer to our model including three compartments, namely naive macrophages, activated macrophages and IL-6 blood concentration (Fig. 1c, equations (8-10)). We focus our attention on IL-6 as more time course data is available.

The main assumption of the model is that macrophage activation is driven by three different, well-described mechanisms: (i) the release of DAMPs by the killing of tumor cells, (ii) the release of inflammatory signals by CAR-T cells upon antigen recognition, and (iii) the contact of activated macrophages and CAR-T cells through the CD40-CD40L axis. In our model we further assume basal influx/production and death/decay rates for monocytes and cytokines, and that IL-6 is released by activated macrophages. We collected additional IL-6 time courses for a subset of 15 patients for which also CAR-T cell time

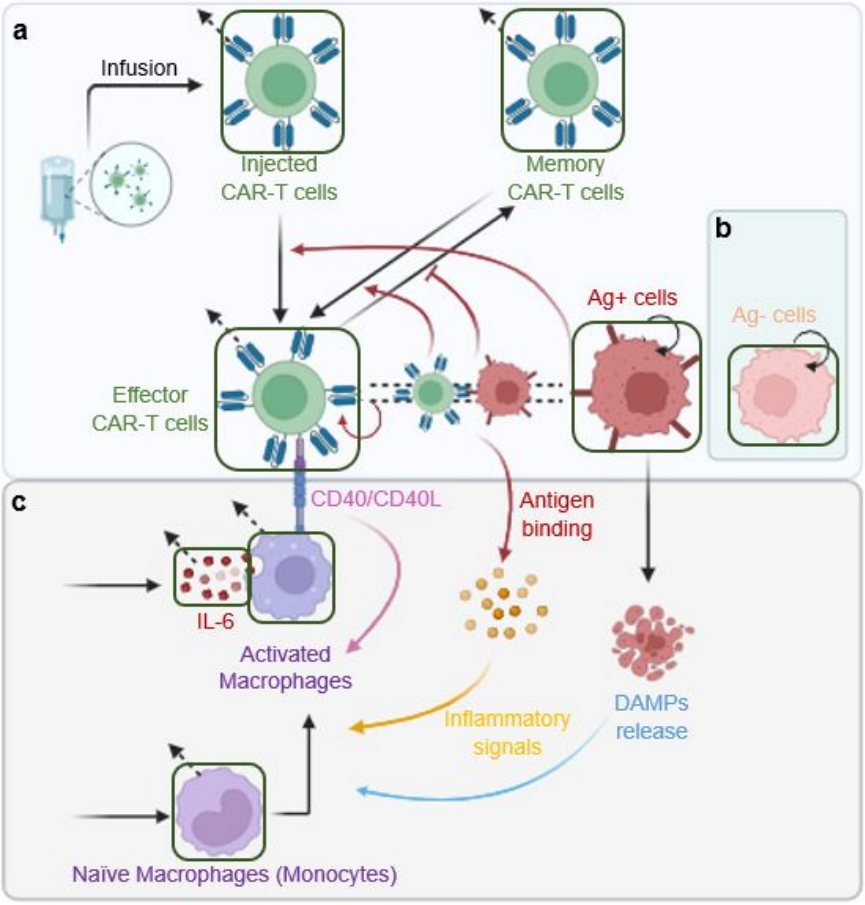

Fig. 1 Model schematic description. **a** Model for CAR-T cell therapy considering injected (C_I), effector (C_E), and memory (C_M) CAR-T cells, and antigen-positive (Ag+) tumor cells (T_P). The phenotypic differentiation of CAR-T cells is driven by antigen recognition on the surface of tumor cells (red arrows). **b** The model is extended to describe patients who presented antigen-negative tumor relapses by including a compartment of antigen-negative (Ag-) tumor cells (T_N). **c** The same model can be extended to describe macrophage-mediated cytokine release considering three different activation mechanisms: antigen-binding (upon antigen-recognition, activated CAR-T cells release inflammatory cytokines and molecules that activate naive macrophages, yellow arrow); DAMPs-release (CAR-T-mediated killing of the tumor leads to the release of damage-associated molecular patterns (DAMPs) that promote monocyte activation, blue arrow); CD40-contact (in a contact-dependent manner, activated macrophages expressing CD40 bind to CD40 ligand expressed by CAR-T cells and promote further macrophage activation (pink arrow). See Methods for model equations.

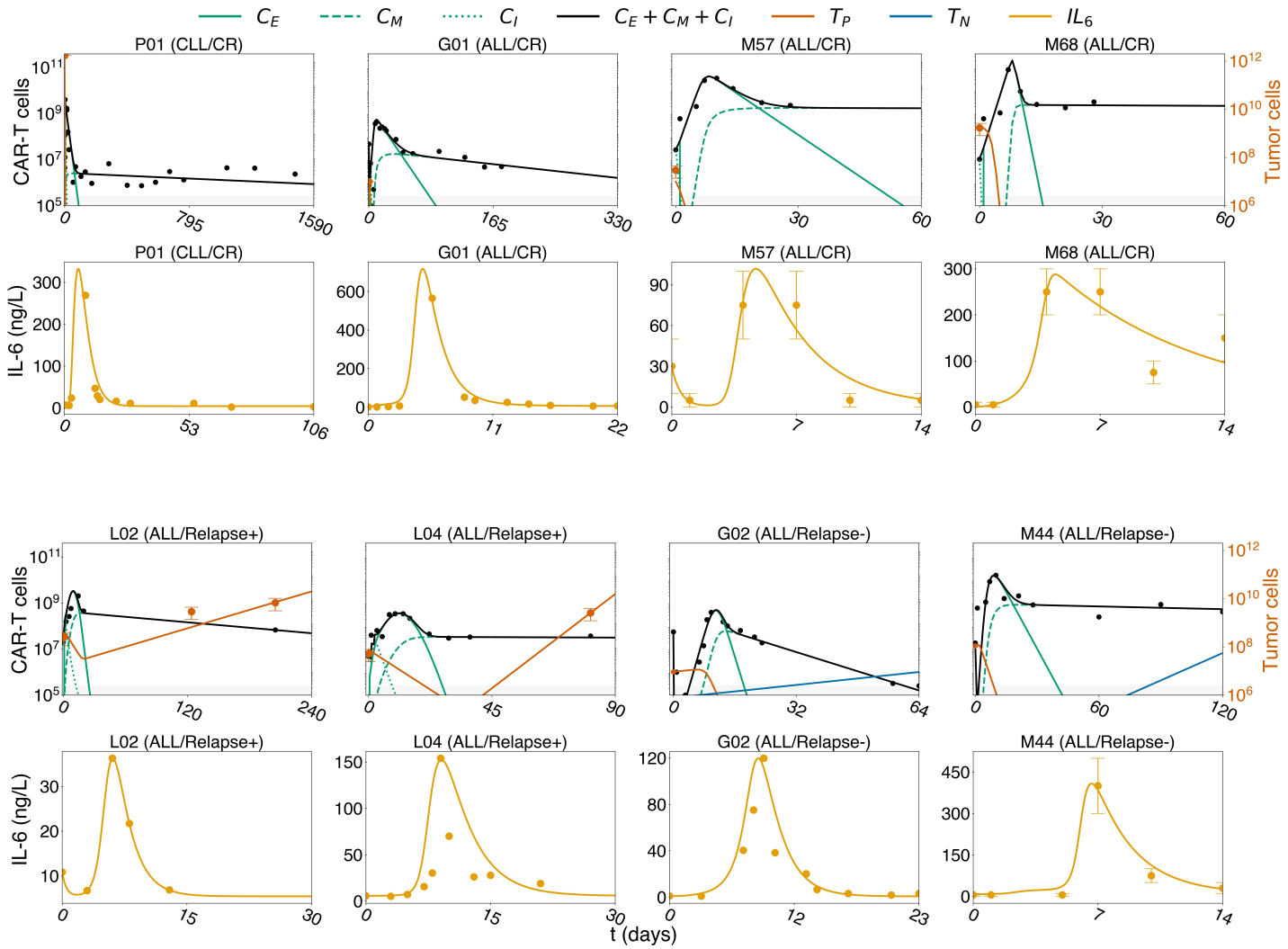

Fig. 2 Model simulations. Model fits for selected patients that showed response to therapy (P01, G01, M57, and M68) or relapse either of antigen-positive tumor cells (L02, L04) or antigen-negative tumor cells (G02, and M44). See Supplementary Figs. 1–4 for all 25 patients and Methods for detailing on the datasets. Although patients M57 and M68 were simulated until their PFS day, plots show their dynamics for 60 days for clarity. Tumor cell error bars represent the range of WBCs used in scaling while error bars for IL-6 in patients M44, M57, and M68 encompass the range reported in [27]. The CAR-T cell detection threshold of 2.5×10^5 cells is represented by the gray shaded area.

courses were available. The model is fitted with excellent agreement between data and simulations (Fig. 2, Supplementary Fig. 4).

We conclude that our modular model structure accurately describes the main dynamical aspects of CAR-T cell therapy, explicitly accounting for CAR-T cell multiphasic dynamics, antigen-positive and negative relapses, and the occurrence of macrophage-mediated CRS.

Different functional mechanisms shape the dynamics of therapy response

The response to CAR-T cell therapy unfolds over time, characterized by distinct phases in CAR-T cell dynamics. Mathematical approaches are suited to identify the functional mechanisms driving each response phase [5]. The fact that after CAR-T cell infusion, both CAR-T and tumor cell numbers change rapidly over different orders of magnitude translates into mathematical arguments allowing to simplify the model equations for each phase and identify leading order effects (see Methods). In brief, each phase is approximated by an exponential function which on the logarithmic scale presents as a straight line with characteristic slopes related to different mechanistic parameters and reflecting patient-specific values (Fig. 3).

Comparing the the slopes calculated from the model fits with the mechanistic parameter responsible for each exponential phase, our analysis shows that the four phases of CAR-T cell dynamics are driven by distinct mechanisms and cellular phenotypes (Fig. 3a-e). The distribution phase is dominated by the decay of injected CAR-T cells, with the slope closely correlated to their death rate $-\mu_I$. This implies that the death rate $-\mu_I$ is the main parameter determining the distribution phase. The subsequent expansion phase is driven by effector CAR-T cells and presents a slope correlated to the net effect between their expansion and reduction due to death and exhaustion, represented as $\kappa - \mu_E$. The contraction phase is characterized by the exhaustion and death of effector CAR-T cells, with slope correlated to their depletion rate $-\mu_E$. The final persistence phase is dominated by the presence of residual long-lived memory CAR-T cells, with slope closely correlated to their death rate $-\mu_E$.

We also identify three phases for tumor responses (Fig. 3f-h). The first is a short and sometimes missing transient phase characterized by tumor growth while the injected CAR-T cells are being activated. Its slope is correlated to the tumor growth rate ρ. The second phase is the shrinkage phase, characterized by a strong decay in the tumor burden due to the CAR-T-mediated killing. Its slope is correlated to the difference between the tumor growth rate and CAR-T cytotoxic effect, $\rho - \gamma$. The last phase is the response phase, which may be either a re-expansion leading to relapse with slope closely correlated to the tumor growth rate ρ, or tumor extinction. The final outcome depends on an intricate balance of all pro and anti-tumor parameters and whether or not the CAR-T cell-mediated killing reduced the tumor burden below a residual disease level.

The identification of model parameters driving the various phases of therapy response in clinical data not only enhances our mechanistic understanding but also proves indispensable for model fitting. As we demonstrate below, the model fitting is further complemented by identifying other parameters governing shape features of the model solutions.

In summary, we could successfully and uniquely link the different phases of the CAR-T and tumor cell response to the underlying mechanistic parameters of our mathematical model.

Sensitivity analysis of CAR-T cell expansion and tumor reduction enables informed parameter estimation

The preceding analysis enhances our understanding of the multiphasic dynamics following CAR-T cell administration. However, it does not elucidate additional shape features of therapy response, such as the CAR-T cell peak height, persistence level, and minimum tumor burden achieved by therapy, and how they correlate with model parameters. To address this question, we conduct a qualitative

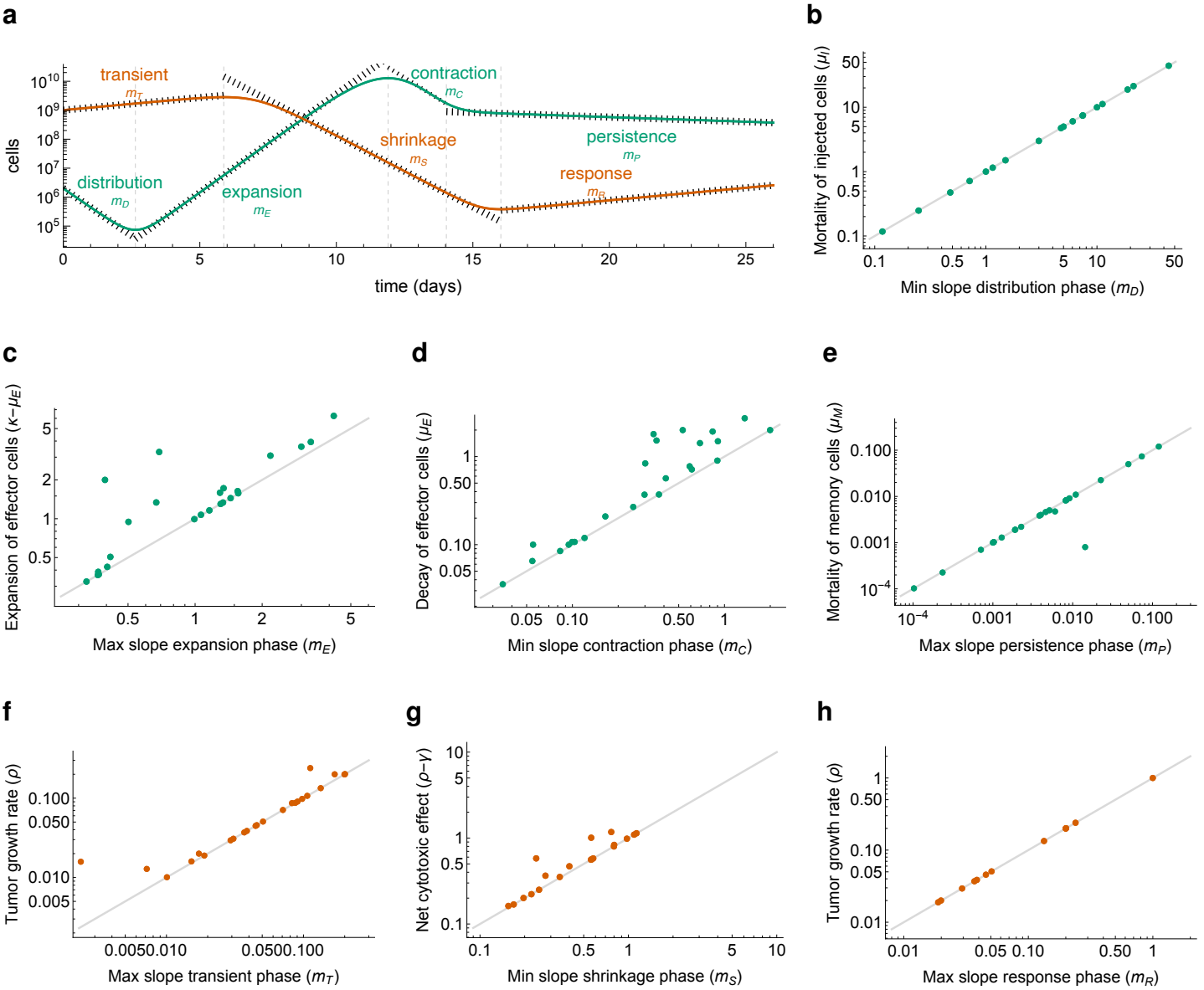

Fig. 3 Identifying mechanisms driving therapy phases. **a** For each patient model fit, the distinct phases for CAR-T (green) and tumor (red) cell responses are identified and the characteristic slope is calculated and compared with the patient-specific mechanistic parameter driving the corresponding phase. **b-h** Comparison between the calculated slope and the mechanistic parameter for each phase and each patient. **b** Distribution phase: the calculated slope is the minimum (negative) slope of CAR-T cells, the mechanistic parameter is $-\mu_I$. **c** Expansion phase: the calculated slope is the maximum (positive) slope of CAR-T cells, the mechanistic parameter is $\kappa - \mu_E$. **d** Contraction phase: the calculated slope is the minimum (negative) slope of CAR-T cells, the mechanistic parameter is $-\mu_E$. **e** Persistence phase: the calculated slope is the maximum (negative) slope of CAR-T cells, the mechanistic parameter is $-\mu_M$. **f** Transient phase: the calculated slope is the maximum (positive) slope of tumor cells, the mechanistic parameter is ρ. **g** Shrinkage phase: the calculated slope is the minimum (negative) slope of tumor cells, the mechanistic parameter is $\rho - \gamma$. **h** Response phase: the calculated slope is the maximum (positive) slope of tumor cells for relapse patients only, the mechanistic parameter is ρ.

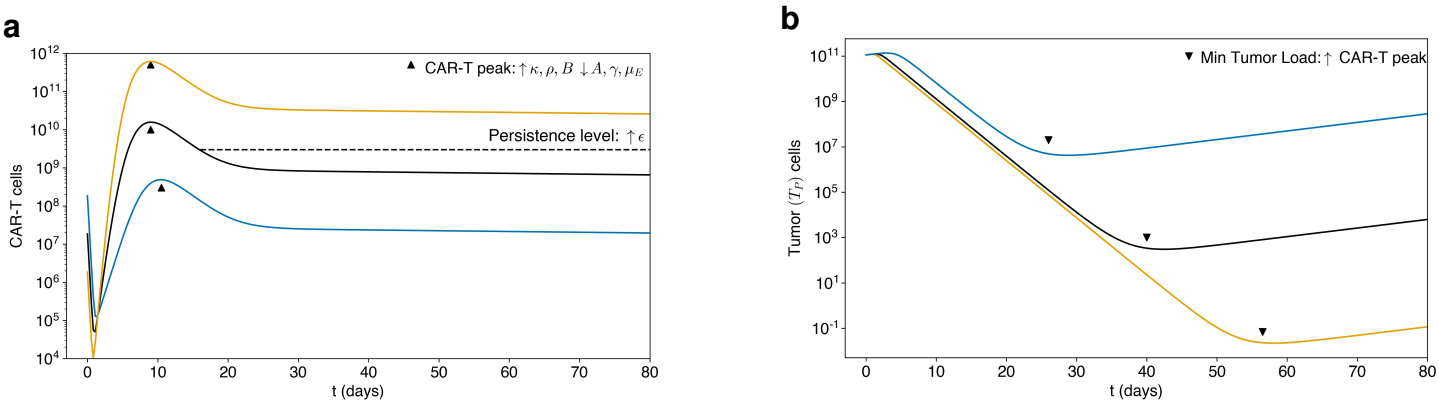

Fig. 4 Qualitative sensitivity analysis. Black curves represent the fitted dynamics, blue curves represent an alternative scenario where CAR-T cells expand less with faster tumor escape, while yellow curves represent a scenario where CAR-T cells underwent greater expansion together with a faster shrinking tumor. Upside triangles indicates CAR-T cells peak and downside triangles indicates the minimal tumor load during therapy. **a** The CAR-T peak level correlates positively with the CAR-T cell expansion rate κ, tumor growth rate ρ, and saturation constant for tumor-killing B, and negatively with tumor kill rate γ, mortality of effector CAR-T cells μ_E, and saturation constant for the antigen-binding function A. The persistence level correlates with the memory formation rate ϵ. **b** The minimum tumor burden is negatively correlated with the CAR-T cell peak. See also Supplementary Figs. 5 and 6.

sensitivity analysis to assess the effect of model parameters on these important response hallmarks (Fig. 4, Supplementary Figs. 5 and 6).

We identified that the parameters primarily influencing the CAR-T cell peak height include the expansion rate of effector cells κ, the tumor growth rate ρ, and the half-saturation constant for tumor-killing functional response B, all exhibiting positive correlations. Conversely, we observed negative correlations with the cytotoxic kill rate of CAR-T cells on tumor cells γ, the mortality of effector CAR-T cells μ_E, and the half-saturation constant for the antigen-binding function A. The minimum tumor burden achieved over time is influenced by the same parameters affecting the CAR-T cell peak (with higher peaks associated with lower tumor burdens). Thus, the expansion of CAR-T cells and the response of tumors are influenced by both product and patient-related characteristics. These include the densities of antigens in tumor cells and receptors in CAR-T cells, related to A and B, respectively. Regarding the CAR-T cells persistence level, we observed a positive correlation with the height of the CAR-T cell peak itself (along with the parameters governing its level) and the memory formation rate ϵ.

This sensitivity analysis, coupled with the previous analysis of the parameters driving each response phase, provides the basis for a step-wise parameter estimation approach. In brief, we found that 10 shape features of model solutions, comprising 7 slopes and 3 max/min points, are mapped on 10 out of 12 parameters of the basic model. The two remaining parameters are the tumor carrying capacity K and the memory recruitment rate θ that can be freely adjusted to the time courses of CAR-T and tumor cells. Based on these findings, we formulate a fitting strategy (see Methods) that utilizes the clinical time courses to derive initial estimates for the 10 parameters. Subsequently, we employ an optimization algorithm to obtain optimal model fits for each available patient (Fig. 2). The efficacy of this strategy underscores the intimate relationship between the shape of the model solutions and the model parameters. Our model can thus be regarded as a minimal model for delineating multiphasic responses.

In conclusion, we demonstrated how distinct model parameters dictate the shape of CAR-T and tumor cell response, providing a systematic approach for parameter estimation and revealing minimal redundancy in the model parameters.

Clinical data suggests poor predictive value of patient-specific factors on IL-6 fold change, but strong temporal connection

So far we illustrated how each feature of the dynamical therapy response corresponds to distinct functional parameters of our model. However, it is well established that certain pharmacological and clinical factors such as CAR-T cell dose, CAR-T cell peak height and time, and initial tumor burden are associated with therapy response or can serve as indicators of severe side-effects [29, 30, 31]. Our modeling approach allows to systemically correlate quantitative estimates of these factors with predicted clinical outcomes. Therefore, for each fitted patient time course, we evaluated and correlated key parameters such as the fold change in IL-6 concentration from baseline to peak, the fold change for CAR-T cell counts from dose to peak, exact peak times for CAR-T cells, IL-6, and macrophages, as well as the tumor burden at days 28 and 90 (Fig. 5).

Our analysis revealed that, for the given cohort of 15 patients, the fold change in IL-6 concentration cannot be correlated with or predicted from the individual patient level based on clinical factors such as total CAR-T cell dose, initial tumor burden, CAR-T cell fold change, or time of IL-6 peak (Fig. 5a-d). This highlights that, on the patient level, the occurrence of CRS, primarily associated with the increase of IL-6 concentrations, does not depend solely on any of the aforementioned factors but appears to emerge from an interplay of various patient-specific factors.

Although no single marker for IL-6 fold change was found, our analysis unveiled a strong temporal connection between events after CAR-T cell infusion (Fig. 5e-f). The estimated CAR-T cell peaks occur within 0 to 5 days after the cytokine peak for almost all patients, aligning with clinical observations [8]. Additionally, the cytokine peak was typically preceded by a peak of activated macrophages occurring 0 to 2 days earlier for all recorded patients. This suggests that CRS might be better predicted by monitoring the levels of activated macrophages. Although these findings need clinical validation they open a window of opportunity to intervene before a critical cytokine peak is building up, thereby lowering the risk of CRS.

We also investigated the remission level at days 28 and 90 post-therapy initiation and assessed their correlation with CAR-T cell expansion (Fig. 5g-i). Neglecting the patients who achieved sustained remission, we observe a negative correlation between tumor burden and CAR-T cell fold change from dose to peak. Although this correlation is robust at day 28, it is less clear by day 90. Instances of patients shifting response status from complete or partial remission at day 28 to different statuses at day 90 (L01, L04, L06, L07, P02) underline the complex dynamic nature of therapeutic outcomes over time. Nevertheless, the direct correlation confirms an association between responses at days 28 and 90.

In summary, while no single marker at the patient level reliably predicts the IL-6 peak and subsequent CRS occurrence, monitoring macrophage levels enables prediction of cytokine kinetics, thereby suggesting a potential clinical intervention.

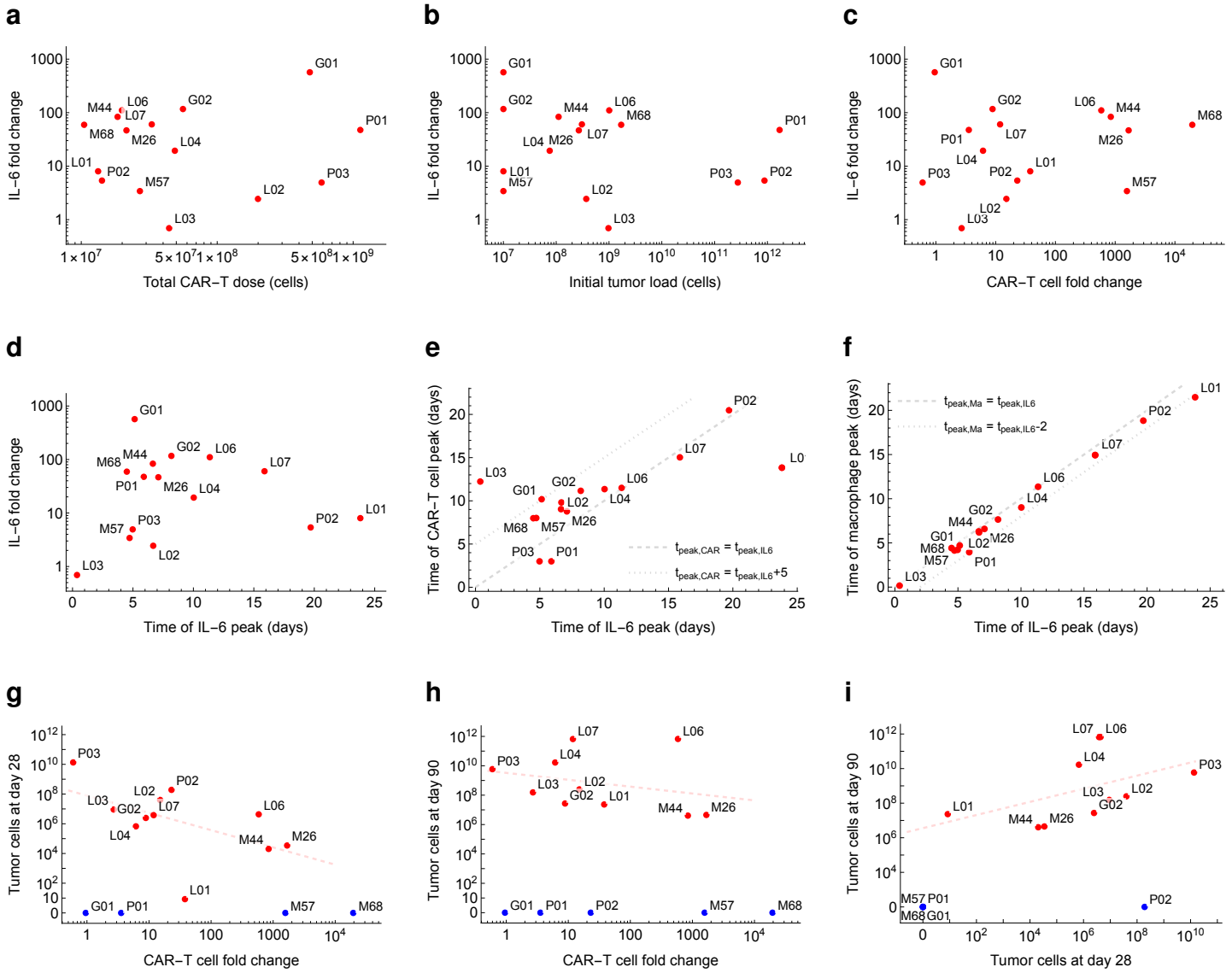

Fig. 5 Patient-specific pharmacological and clinical parameters evaluated from model fits. a-d Within the patient-level, the fold change in IL-6 concentration (baseline to peak) can not be predicted from a single indicator, such as total CAR-T dose, initial tumor burden, CAR-T cell fold change (dose to peak), or time of IL-6 peak. **e** However, for the majority of patients, the model predicts that the peak of CAR-T cells occur between 0 and 5 days after the cytokine peak (dashed lines). **f** For all patients, the cytokine peak is predicted to occur between 0 and 2 days after the peak of activated macrophages (dashed lines). **g** excluding patients predicted to present complete remission at day 28 (blue dots, patients G01, P01, M57, M69), the tumor burden at day 28 after therapy start is negatively correlated to CAR-T cell fold change. This correlation is given by $\log_{10}(T_{28}(x)) = 7.90 - 1.16x$ (dashed line), where $x = \log_{10}(C_{peak}/C_{dose})$, meaning that for each 10-fold increase in the CAR-T cell population, the tumor burden at day 28 is likely to decreases 1.16 logs. **h-i** The correlation is weaker at day 90 since some patients with good/partial response at day 28 loose it at day 90 (L04, L06, L07) while a patient with a partial response at day 28 presented a good response later (P02); with exception of these cases, the model predicts a moderate association between responses at days 28 and 90.

CAR-T cell dose and initial tumor burden influence individual treatment outcome

We showed that two crucial and clinical available parameters, namely CAR-T cell dose and initial tumor burden are insufficient to individually predict the severity of potential side effects, reflected by the poor correlation with IL-6 fold change. However, in terms of our mathematical model we can evaluate how changes of these parameters effect treatment outcome on a cohort level. Using the optimal parameter set identified for each patient and changing only the CAR-T cell dose or initial tumor burden, we study how a 10 and 100 fold change in these parameters affect typical response parameters, including CAR-T cell peak height, remission levels and memory formation at days 28 and 90, IL-6 fold change (baseline to peak), and time points of CAR-T cell and IL-6 peaks (Fig. 6).

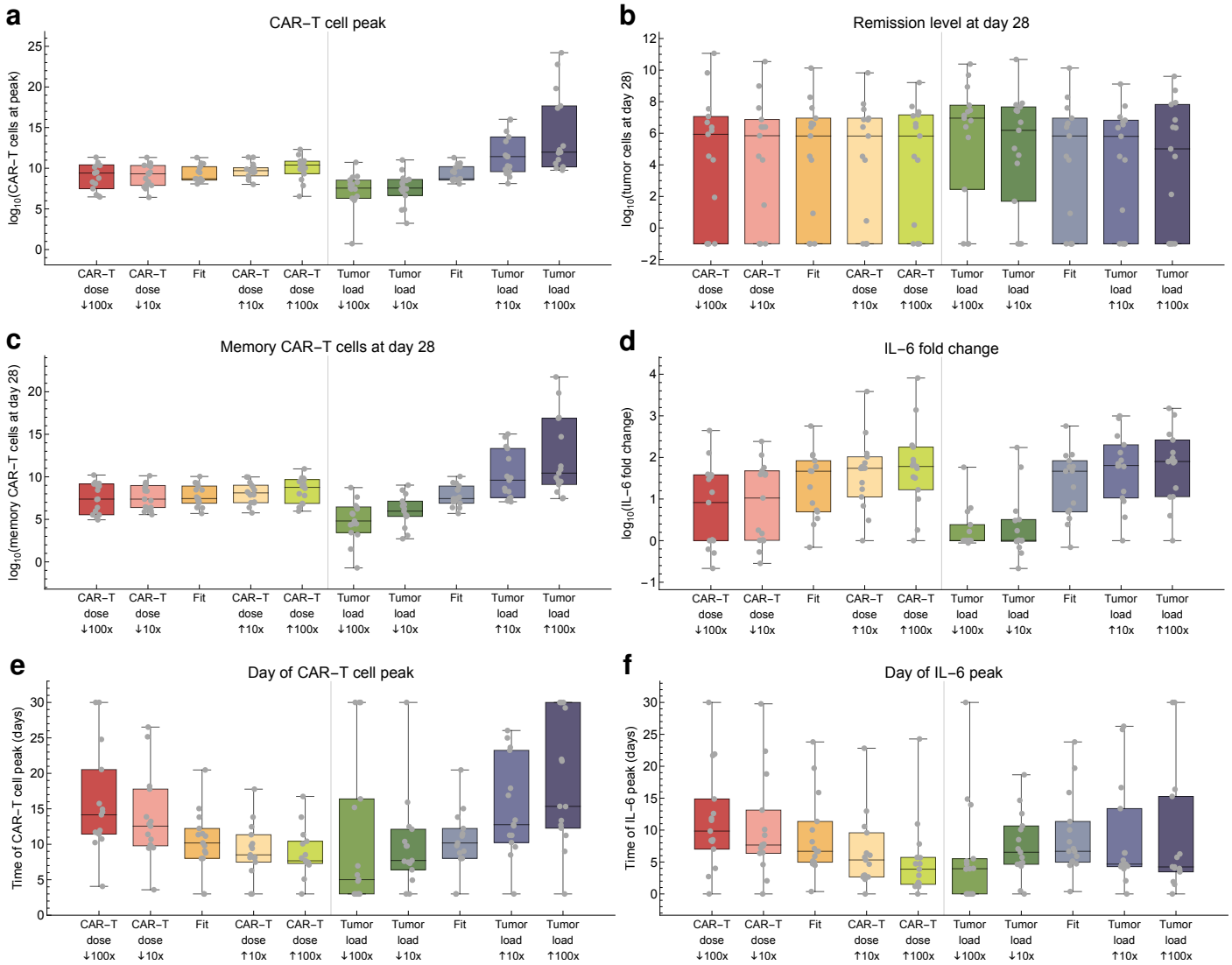

Fig. 6 Effect of different dosing protocols on CAR-T cell dynamics, tumor response, and cytokine peak. To investigate the outcomes of a different CAR-T dose or change in the preconditioning or bridging therapy, we compared the standard scenario (Fit) with simulations starting with either a different CAR-T dose or initial tumor burden (10x and 100x smaller and higher). Assessed outcomes were: **a** number of CAR-T cells at peak, **b** number of tumor cells at day 28, **c** number of memory CAR-T cells at day 28 **d** IL-6 fold change (baseline to peak), **e** day of CAR-T cell peak, **f** day of IL-6 peak. The number of tumor and memory CAR-T cells at day 90 were also assessed and did not present significant differences (Supplementary Fig. 7).

Upon analyzing the impact of different CAR-T cell doses, we observed that the expansion of CAR-T cells, remission levels and memory formation at days 28 and 90 remained almost unaffected (Fig. 6a-c). However, smaller doses resulted in decreased IL-6 fold change and delayed CAR-T cell and IL-6

peaks (Fig. 6d-f). This suggests that smaller CAR-T cell doses extend the expansion phase without a proportional increase in absolute cell numbers, maintaining overall remission levels. Moreover, this extended CAR-T cell expansion phase potentially leads to a more distributed activation of macrophages over time, as reflected not only in the delayed IL-6 peak but also in a decreased fold change from baseline to peak, potentially reducing the chances of severe CRS.

Initial tumor burden is an important factor that can be targeted in a clinical context during bridging and preconditioning therapy. Decreasing the initial tumor burden, we noted a reduction in both CAR-T cell peaks and IL-6 fold (Fig. 6a,d) with an early CAR-T cell peak and no significant alterations for the IL-6 peak time (Fig. 6e-f). Additionally, modifying the initial tumor burden resulted in minimal changes in remission levels at days 28 and 90, but higher tumor burdens were linked to increased memory formation (Fig. 6b-c).

Although we see a correlation between IL-6 peak levels and both the CAR-T cell dose and the initial tumor burden (Fig. 6d), this effect is not proportional as it would be expected from a naive approach. It rather appears that a saturation arises from the functional model setup in which antigen-binding and DAMPs serve as a trigger rather than the primary mechanism for macrophage activation (see below).

It is worth noting that important parameters regarding long-term response (namely remission level and memory formation) are not influenced by changes in the initial CAR-T dose, while a lower initial tumor burden does not affect remission level but leads to less memory formation. Moreover, side effects due to cytokine release could potentially decrease with smaller administered CAR-T cell doses and intensive pre-conditioning to reduce the initial tumor burden.

In conclusion, our findings suggest that adjusting the administered CAR-T cell dose may exert a greater influence on kinetic parameters such as peak times and IL-6 peak height. The initial tumor burden and the corresponding antigen load appears to serve as a catalyst for CAR-T cell expansion, potentially explaining higher persistence of CAR-T cells but also increased severity of cytokine-related side effects.

Disentangling mechanisms of macrophage activation and CRS timeline

While it appears that cytokine-related side effects can be reduced by adjusting CAR-T cell dose or initial tumor burden, targeting macrophage-mediated cytokine release directly is also a clinical option. A quantitative understanding of the temporal dynamics of macrophage activation and cytokine release is crucial for this purpose.

Our model assumes three distinct molecular and cellular mechanisms for macrophage activation, namely DAMPs release, antigen-binding, and CD40 contact, described by parameters β_K, β_B and β_C respectively (equation (11)). To unveil the dynamics underlying these mechanisms, we simulated the time course of patient M44, selectively activating one mechanism at a time (Fig. 7a). Activation via DAMPs release alone ($\beta_K > 0$, $\beta_B, \beta_C = 0$) led to IL-6 peak around day 3, during the tumor shrinkage phase. Activation solely through antigen recognition ($\beta_B > 0$, $\beta_K, \beta_C = 0$) resulted in IL-6 concentration rising concurrently with CAR-T cell expansion, peaking around day 8. Considering only CD40-mediated activation ($\beta_C > 0$, $\beta_K, \beta_B = 0$), IL-6 kinetics remained at baseline levels due to the requirement of previous infiltration by naive macrophages. Yet, integrating CD40-mediated activation with small values for DAMPs release and antigen-binding parameters ($\beta_K >> 0$, $\beta_B, \beta_C \approx 0$), the IL-6 peak occurred around day 13, four days post-CAR-T cell peak (purple curve). These findings suggest that each mechanism occurs at distinct time points, influenced by various interactions unfolding after infusion: DAMPs drive macrophage activation during the tumor shrinkage phase, followed by antigen-binding-mediated activation during CAR-T cell expansion, and contact-dependent CD40-mediated activation.

To understand the individual contributions of each mechanism, we divided the activated macrophages into three sub-populations based on their source (DAMPs-activated, antigen-activated, CD40-activated) and, for each patient, determined the peak time and cumulative number of activated macrophages for

each sub-population, and the CAR-T cells and IL-6 peak times (Fig. 7b). Interestingly, the previously described timeline holds true for the majority of patients: DAMP-activated macrophages reach their peak levels first, followed by the peak of antigen-activated macrophages, followed by the peak of CD40-activated macrophages.

While all these mechanisms theoretically could equally contribute to macrophage activation, a computation of the cumulative number of activated macrophages in each sub-population revealed that the CD40 contact-dependent mechanism accounts for the majority of activated macrophages (pie charts in Fig. 7b). This intriguing discovery suggests that macrophage activation mediated by contact-independent mechanisms, such as DAMPs release and the release of GM-CSF and IFN-γ by antigen-binding-activated CAR-T cells, is limited and may not be the primary source of inflammation and CRS. On the contrary, our findings propose that once CD40-mediated activation is triggered by previous mechanisms, it enters a feedback loop in which activated macrophages in contact with CAR-T cells further activate more macrophages, leading to massive cytokine release. These results confirm that CD40–CD40L interactions are not essential for eliciting cytokine release but are likely the primary drivers exacerbating macrophage activation, IL-6 production, and CRS severity.

In summary, our findings indicate that macrophage activation via DAMPs release, antigen-binding, and CD40 contact unfolds sequentially during therapy, with CD40-mediated inflammation playing a predominant role.

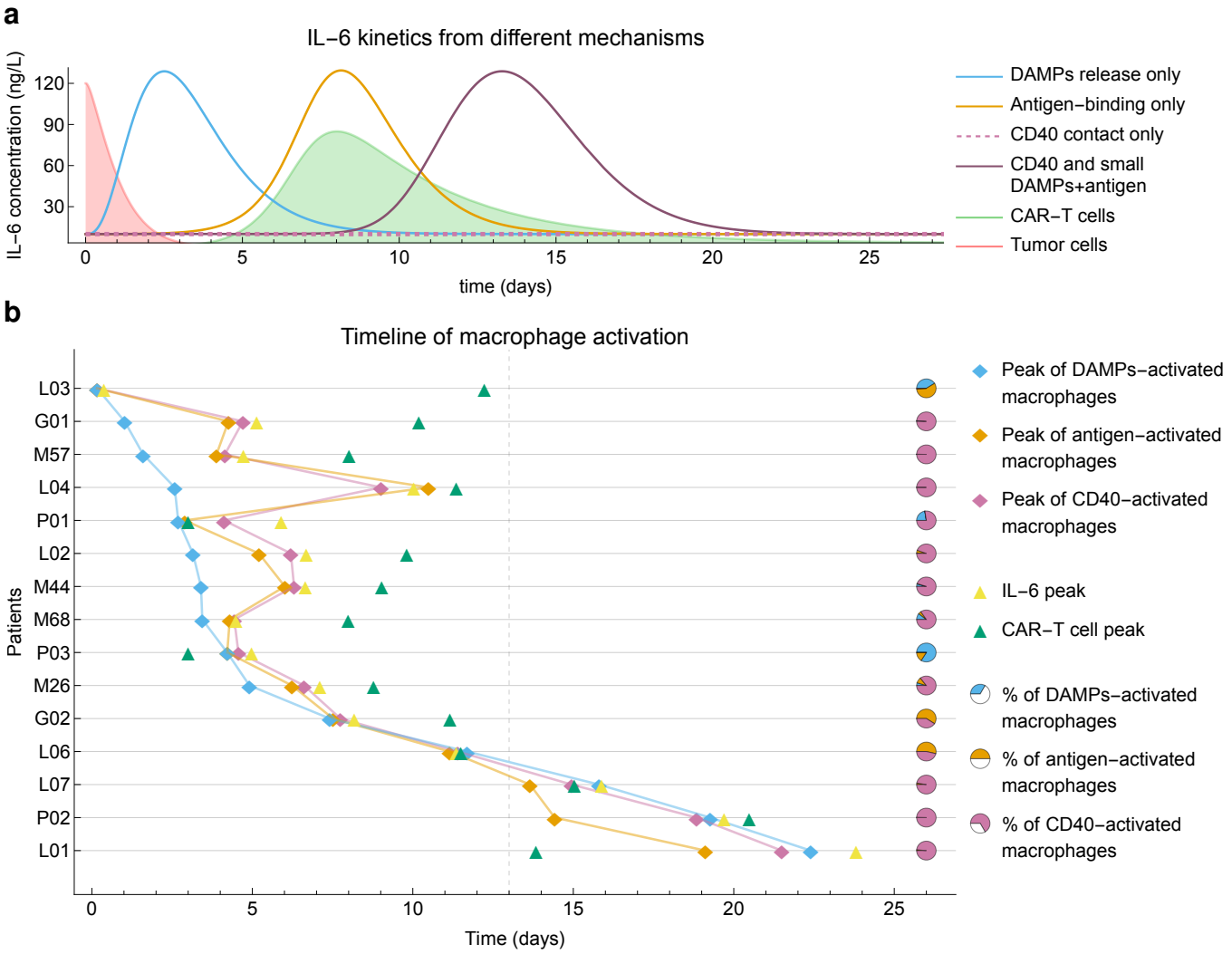

Fig. 7 Dynamics of macrophage activation and cytokine release. **a** Time course of patient M44, selectively activating DAMPs release, antigen-binding, and CD40 contact mechanisms one at a time. DAMPs-only activation leads to an IL-6 peak around day 3 during tumor shrinkage. Antigen-biding activation results in IL-6 increasing with CAR-T expansion, peaking around day 8. CD40-mediated activation alone maintains IL-6 at baseline, but when combined with small values for DAMPs and antigen-binding parameters, it produces an IL-6 peak around day 13, four days after the CAR-T cell peak. **b** Splitting the active macrophage population according to their source, i.e., activation mechanisms (see Methods), and reconstructing the timeline for each patient, we found that the peak of DAMP-activated macrophages takes place early, during the tumor shrinkage phase. The second subpopulation to present a peak is the antigen-binding-activated macrophages, which expand in parallel with CAR-T expansion. The last sub-population to peak are CD40-activated macrophages, which require the presence of previously activated macrophages. For 11 out of the 15 patients, the major source of activated macrophages was CD40 contact (pie charts).

Targeted interventions to control macrophage activation

The deconvolution of the different mechanisms driving macrophage activation hints towards a clinical intervention to mitigate CRS. Currently, the primary drug used to address CRS is Tocilizumab, a monoclonal antibody that acts as an IL-6 antagonist [12]. However, targeting macrophage activation with GS-CSF and CD40 antibodies has also been explored in cell-based studies [32].

To mimic the use of such antibodies that specifically inhibit macrophage activation, we applied our patient-specific model but reduced the parameters related to macrophage activation, β_K, β_B and β_C one at time (Fig. 8a). We observe that the IL-6 peak decreased with increased blocking, with varying effects depending on the patient. Overall, for a 50% reduction in the respective activation parameter, the mean reduction in the IL-6 peak was 5%, 9%, and 42% for DAMP, antigen-binding, and CD40, respectively. This confirms that the CD40-CD40L interaction is not only a major driver of CRS but also a promising target for clinical interventions.

To demonstrate the clinical potential of CD40 blocking, we conducted a series of model simulations reducing, for each patient, the CD40 parameter to 50% of the original value starting at different time points after infusion and keeping the block until either before, at or after the CAR-T cell peak (Fig. 8b). We found that initiating the blocking 1 or 2 days after CAR-T cell infusion is most effective, with the block being maintained until or after the CAR-T cell peak. On average, a 30-40% reduction in IL-6 peak can be achieved with some patients showing even stronger responses.

Our model of sequential macrophage activation demonstrates that targeting the CD40-CD40L axis is the most effective and clinically feasible strategy to control macrophage activation and reduce IL-6 peak height.

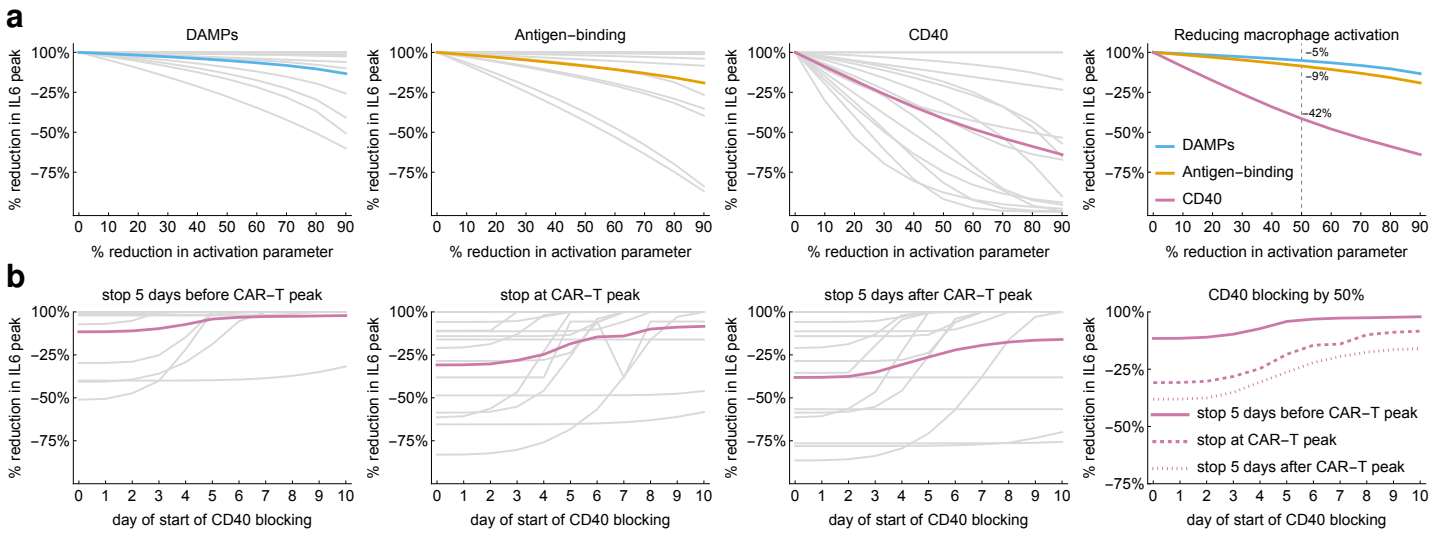

Fig. 8 Blocking of macrophage activation and cytokine release. a Simulation results of interventions reducing mechanisms of macrophage activation one at a time, showing the reduction in IL-6 peak for each patient (gray curves) and mean effect (colored curves). For a simulated 50% reduction (dashed line, fourth panel) the overall reduction in IL-6 peak is indicated for each mechanism. **b** Simulation results of interventions blocking CD40 starting 0-10 days after CAR-T cell infusion, stopping -5, 0 and 5 days after CAR-T cell peak. The plots show the resulting reduction in IL-6 peak for each patient (gray curves) and the mean effect (colored curves).

Discussion

We developed a novel multi-layer mathematical model to investigate tumor response and CRS following CAR-T cell immunotherapy. The model accurately describes the timeline of therapy response and relates its dynamic shape to interpretable model parameters. Our findings highlight the role of early macrophage activation in cytokine release, thereby outlining potential strategies for clinical monitoring and prevention of CRS. By disentangling different modes of macrophage activation we identified the CD40-CD40L axis as a clinically feasible target to control the activation process and modulate IL-6 peak height.

The diverse configuration and clinical outcomes of patient responses to CAR-T cell therapy is attributed to product- and patient-specific factors [29]. Our model unveiled the mechanisms underlying multiphasic therapy response, showing how each of its shape features is linked to a specific model parameter. While, on one hand, this close correlation is the basis for a model-informed step-wise parameter estimation strategy, it, on the other hand, explains how key clinical indicators (CAR-T cell peak, persistence, and minimal tumor burden) are modulated by product-related factors (CAR-T cell expansion, cytotoxicity and receptor density) and patient-specific variables (tumor growth rate and antigen density). In particular, the modeled persistence level of memory CAR-T cells is positively correlated to the CAR-T peak level, in line with recent findings that patients with positive ddPCR (indicative for persistence) at six months had a significantly higher median peak of CAR-T cell copies compared with negative ddPCR [33]. Also, the minimal tumor burden is inversely related to the CAR-T cell peak level, consistent with [34], which reported that higher peaks of CAR-T cells within 15 days are associated with increased likelihood of achieving complete remission.

While the precise determinants of CRS severity remain debated, existing literature suggests that initial tumor burden and CAR-T cell dose correlate with CAR-T cell peak height [30, 31]. In a study with 237 patients, severe CRS strongly correlated with high tumor burden but not with CAR-T cell dose [35]. In our patient-level analysis, neither CAR-T cell dose nor initial tumor burden reliably predicted IL-6 increase (as a surrogate for CRS severity) a priori. However, cohort simulations with varying CAR-T cell dose and tumor burden shows that smaller CAR-T cell doses reduced IL-6 fold, potentially lowering severe CRS risk without significantly affecting CAR-T cell peak, remission levels, or memory formation. Decreased initial tumor burdens also reduced IL-6 levels but lowered both CAR-T cell peak and persistence, with minimal impact on remission levels. In summary, predicting CRS occurrence a priori at the patient level is still challenging, while modulating dose or initial tumor burden offer potential for optimizing therapeutic outcomes.

Mouse models showed that CRS involves a multicellular network comprising CAR-T and host cells, with macrophages playing a crucial role [14, 16]. A recent review [8] proposes that macrophage-mediated CRS emerges from antigen-binding-mediated inflammation, DAMPs release and CD40 contact. Built upon these concepts, our model accurately replicates these dynamics, showing an early peak of activated macrophages followed by cytokine peak within 1-2 days, then a CAR-T cell peak within 1-5 days. Disentangling these mechanisms, we showed that DAMPs underlie early cytokine release, while antigen-binding drives cytokine increase parallel to CAR-T cell expansion, and CD40 contact leads to late cytokine rise. A deeper analysis indicates that CD40 is the latest but the main driver of macrophage activation, suggesting that antigen-binding and DAMPs act more as triggers than primary mechanisms.

The preponderant role of CD40-contact in macrophage activation poses a candidate for interventions against CRS. Simulating a reduction of the different activation mechanism showed that targeting CD40 leads to the most substantial reduction in IL-6 peak height, causing an average reduction of 42% in the case of constant blocking and 30% reduction when blocking from day 2 after infusion to 1 day after CAR-T cell peak. This aligns with a recent cell-based in vitro model for CRS that showed that IL-6 supernatant levels decreased 20-30% when blocking cytokine release by bystander macrophages with neutralizing antibodies for GM-CSF and CD40, and decreased 30–40% due to the genetic disruption of

the CD40L and/or CSF2 knock-out CAR-T cells [32].

While our model provides insights on therapy response and macrophage-mediated CRS, it also faces limitations. The one-to-one correspondence between parameters and time course shape features allows parameter identification but requires tumor data at several time points, which is not available in most cases [27, 1, 36, 37, 38]. Although preclinical models indicated that IL-6 plays a role in macrophage activation, the exact degree of this contribution remains uncertain [14]. Due to the need for additional data to accurately calibrate this relationship, we opted not to incorporate a feedback mechanism of IL-6 on macrophage activation, regarding it as a second-order effect. Finally, while we use IL-6 fold increase to indicate CRS severity, there is no standardization in clinical grading scales [39], which are often based on symptoms or therapeutic interventions rather than measurable thresholds [40, 41, 42].

In conclusion, our study demonstrates the efficacy of a compact multi-module mathematical model in accurately describing a retrospective dataset from patients undergoing CAR-T cell therapy. Our findings shed light on the influence of macrophage activation on cytokine release and pinpoint the CD40-mediated mechanism as the primary driver of cytokine release, suggesting it as a potential target for CRS treatment strategies. Moreover, our approach underscores the importance of mechanistic models, revealing how their application to clinical data can unveil and elucidate underlying interactions not immediately apparent. Finally, this work illustrates how precise, clinically-motivated mathematical models can inform patient-specific treatment decisions, emphasizing the need for ongoing integration with evolving clinical data collection efforts.

Methods

Mathematical model

Modeling CAR-T multiphasic dynamics based on phenotypic differentiation and antigen-positive tumor responses

We simplified our previous model [5] into a complete mechanistic system aimed at describing, with minimal number of parameters, the multiphasic dynamics of CAR T-cells as a process emerging from the interaction between CAR-T phenotypes and their binding to antigen-expressing tumor cells. To do so, we incorporated assumptions for T-cell turnover, in which the reaction rate of a T-cell is based on its phenotype - naive cells become active, activated cells expand, and memory cells are re-activated - and is proportional to its binding with antigen-expressing target cells [26]. Our model, consisting of four compartments, accounts for three CAR-T cell phenotypes: injected, effector, and memory cells, represented as $C_D(t)$, $C_E(t)$, and $C_M(t)$, respectively, along with a population of antigen-positive tumor cells denoted as $T_P(t)$. The model is formally given by

$$\underbrace{\frac{dC_I}{dt}}_{\text{Injected CAR-T}} = -\underbrace{\eta F(T_P)C_I}_{\text{Activation}} - \underbrace{\mu_I C_I}_{\text{Death}} \tag{1}$$

$$\underbrace{\frac{dC_E}{dt}}_{\text{Effector CAR-T}} = \underbrace{\eta F(T_P)C_I}_{\text{Activation}} + \underbrace{\kappa F(T_P)C_E}_{\text{Expansion}} - \underbrace{\epsilon(1-F(T_P))C_E}_{\text{Memory formation}} + \underbrace{\theta F(T_P)C_M}_{\text{Memory activation}} - \underbrace{\mu_E C_E}_{\text{Death and exhaustion}} \tag{2}$$

$$\underbrace{\frac{dC_M}{dt}}_{\text{Memory CAR-T}} = \underbrace{\epsilon(1-F(T_P))C_E}_{\text{Memory formation}} - \underbrace{\theta F(T_P)C_M}_{\text{Memory activation}} - \underbrace{\mu_M C_M}_{\text{Death}} \tag{3}$$

$$\underbrace{\frac{dT_P}{dt}}_{\substack{\text{Tumor}\\ \text{antigen-positive}}} = \underbrace{\rho T_P\left(1-\frac{T_P}{K}\right)}_{\text{Tumor growth}} - \underbrace{\gamma\frac{C_E}{B+C_E}T_P}_{\text{CAR-T killing}} \tag{4}$$

The function $F(T_P)$ represents the antigen-receptor biding interaction and is described by a Michaelis-Menten functional response

$$F(T_P) = \frac{T_P}{A+T_P}, \tag{5}$$

where A is the half-saturation constant. Following the approach in [26], we incorporated this function into all transition terms for CAR T-cells. This implies that the *per capita* rates of activation, expansion and memory recruitment are proportional to the antigen-binding function $F(T_P)$, while the rate of memory formation is proportional to $1 - F(T_P)$. The model further assumes decay rates for each CAR-T cell phenotype (μ_I, μ_M), encompassing natural death and exhaustion for effector CAR T-cells (μ_E), and a logistic growth for tumor cells at a rate ρ with a carrying capacity K. Following [43], the killing of tumor cells is described by a Holling type-II response with saturation for the effector cells; which also corresponds to a simplification in our previous model ($\vartheta = 0$) [5]. The Michaelis-Menten functional responses were chosen because it effectively captures the saturating nature of the antigen-receptor binding process, either by the limited number of antigen density in tumor cells (higher values of A) or by receptor density in CAR T-cells (higher values of B). An overview of model parameters is presented in Supplementary Table 1.

Modeling antigen-negative tumor relapse

We expanded the system (1-5) to include antigen negative tumor cells. This was achieved by simplifying our recent PDE model that describes the interaction of CAR T-cells with a heterogeneous population of tumor cells [7]. Instead of single equation (4) for antigen-positive tumor cells, we now have two equations representing antigen-positive (T_P) and antigen-negative (T_N) tumor cells,

$$\underbrace{\frac{dT_P}{dt}}_{\substack{\text{Tumor}\\ \text{antigen-positive}}} = \underbrace{\rho T_P\left(1-\frac{T_P+T_N}{K}\right)}_{\text{Growth}} - \underbrace{\gamma\frac{C_E}{B+C_E}T_P}_{\text{CAR-T killing}} \tag{6}$$

$$\underbrace{\frac{dT_N}{dt}}_{\substack{\text{Tumor}\\ \text{antigen-negative}}} = \underbrace{\rho T_N\left(1-\frac{T_P+T_N}{K}\right)}_{\text{Growth}} - \underbrace{g_0\gamma\frac{C_E}{B+C_E}T_N}_{\text{CAR-T killing}}. \tag{7}$$

The killing of antigen-negative cells is multiplied by a fraction g_0 which represents a reduced cytotoxicity due to antigen absence. We assumed a small, but nonzero value for g_0 to account for a minimal cytotoxic effect by CAR-T cells due to the bystander effect and/or CAR-T cell endogenous TCR [28, 44]. We have also considered that antigen-negative tumor cells do not contribute to CAR-T activation, expansion, and memory recruitment, as these process are dependent on antigen-binding interactions. Therefore, the model for CAR-T cell therapy in a context with antigen-positive and antigen-negative tumor cells is formed by equations (1-3), (5) and (6-7).

Modeling macrophage-mediated cytokine release

In line with widely accepted biological mechanisms [15, 16, 45], we model the kinetics of cytokine concentrations following CAR-T administration, assuming that cytokine release is mediated by macrophage

activation. This activation and subsequent recruitment is driven by three main mechanisms: i) upon target recognition, activated CAR T-cells release cytokines and soluble inflammatory mediators that activate macrophages, such as interferon-γ, granulocyte–macrophage colony-stimulating factor and tumor necrosis factor; ii) the killing of tumor cells releases damage-associated molecular patterns (DAMPs) that further amplify macrophage activation; and iii) macrophage activation is also promoted by a contact-dependent mechanism, through the expression of CD40 and CD40-ligand by macrophages and CART-cells, respectively.

We then assume that activated macrophages secrete inflammatory cytokines, including IL-6, chosen due to its significant role in CRS and the availability of patient time courses containing IL-6 kinetics alongside CAR-T cell responses. Under these assumptions, the model for macrophage activation and cytokine release reads as

$$\underbrace{\frac{dM_i}{dt}}_{\substack{\text{Naive}\\\text{macrophages}}} = \underbrace{\sigma_M}_{\text{Production}} - \underbrace{h(C_E, T_P, M_a)M_i}_{\text{Activation}} - \underbrace{\delta_M M_i}_{\text{Death}} \tag{8}$$

$$\underbrace{\frac{dM_a}{dt}}_{\substack{\text{Activated}\\\text{macrophages}}} = \underbrace{h(C_E, T_P, M_a)M_i}_{\text{Activation}} - \underbrace{\delta_M M_a}_{\text{Death}} \tag{9}$$

$$\underbrace{\frac{dIL_6}{dt}}_{\text{Cytokine}} = \underbrace{\sigma_I}_{\substack{\text{Basal}\\\text{production}}} + \underbrace{\alpha M_a}_{\substack{\text{Release by}\\\text{macrophages}}} - \underbrace{\delta_I IL_6}_{\text{Decay}}. \tag{10}$$

where M_i and M_a represent the naive (monocytes) and activated macrophages, respectively, and IL_6 describes the IL-6 concentration. Furthermore, σ_M is the natural production rate of naive macrophages, δ_M is the death rate of macrophages, σ_I represents the endogenous production rate of IL-6, δ_I is the IL-6 natural decay rate, and α is the rate of IL-6 release by activated macrophages. The macrophage activation rate is given by

$$h(C_E, T_P, T_n, M_a) = \underbrace{\beta_K \frac{C_E}{B + C_E}(T_P + g_0 T_N)}_{\text{Antigen-binding}} + \underbrace{\beta_B \frac{T_P}{A + T_P} C_E}_{\text{DAMPs release}} + \underbrace{\beta_C \frac{M_a}{C + M_a} C_E}_{\text{CD40 contact}} \tag{11}$$

and encompasses the contribution of the three different mechanisms for macrophage activation: antigen-binding-mediated release of inflammatory signals by CAR-T cells (first term, proportional to CAR-T activation, with contribution β_B), tumor-killing-mediated release of DAMPs (second term, proportional to tumor killing, with contribution β_K), and CAR-T cell and macrophages contact (third term, Michaelis-Menten kinetics for CD40-CD40L binding, with contribution β_C).

Approximating solutions and predicted slopes for multiphasic dynamics

In this section, we present the rationale that allows to simplify the ODEs for total CAR-T and tumor cells. This simplification leads to the calculation of approximate solutions for each phase, along with their characteristic slopes. These arguments are supported by a quantitative approach in which, for each patient, we calculated the characteristic slopes from the model solution at each phase and compared them with the predicted parameter governing each slope (Fig. 3).

The total CAR-T cell population is given by $C = C_I + C_E + C_M$ and is described by

$$\frac{dC}{dt} = -\underbrace{\mu_I C_I}_{\text{Injected death}} + \underbrace{\kappa F(T_P) C_E}_{\text{Effector expansion}} - \underbrace{\mu_E C_E}_{\substack{\text{Effector death and}\\\text{exhaustion}}} - \underbrace{\mu_M C_M}_{\text{Memory death}}.$$

During the distribution phase, the CAR T-cell population consists mainly of injected cells, from which we approximate $C \approx C_I$ and $C_E, C_M \approx 0$. Thus, $dC/dt \approx -\mu_I C$, leading to an approximating solution $C = C_0 e^{-\mu_I t}$ with slope $-\mu_I$. During the expansion phase, the tumor burden is high and the CAR-T cell population consists mainly of effector cells, leading to the approximation $C \approx C_E$, $C_I, C_M \approx 0$, $F(T_P) \approx 1$. The approximating ODE is $dC/dt \approx (\kappa - \mu_E)C$, leading to an approximating solution $C = C_{\text{min}} e^{(\kappa-\mu_E)t}$ with slope $\kappa - \mu_E$. Similarly, in the contraction phase the CAR-T cell population presents the same characteristics, but with a reduced tumor burden, leading to $F(T_P) \approx 0$ and $dC/dt \approx -\mu_E C$. The approximating solution reads as $C = C_{\text{max}} e^{-\mu_E t}$ with slope $-\mu_E$. Finally, the persistence phase is characterized by the presence of long-lived memory cells, leading to $C \approx C_M$, $C_E, C_I \approx 0$ and an approximating solution $C = C_{\text{con}} e^{-\mu_M t}$ with slope $-\mu_M$.

Similarly, the total tumor population, given by $T = T_P + T_N$, is described by

$$\frac{dT}{dt} = \underbrace{\rho T \left(1 - \frac{T}{K}\right)}_{\text{Tumor growth}} - \underbrace{\gamma \frac{C_E}{B + C_E}(T_P + g_0 T_N)}_{\text{CAR-T killing}}.$$

During the transient phase, the number of effector CAR-T cells is small and, due to the preconditioning therapy, the tumor burden is far below the carrying capacity. Also, $C_E \approx 0$, and the dynamics is approximated by $dT/dt \approx \rho T$, leading to an approximating solution $T = T_0 e^{\rho t}$ with slope ρ. During the shrinkage phase, the number of CAR-T cells is very high, leading to $C_E/(B + C_E) \approx 1$ while the majority (if not all) of tumor cells is antigen-positive, $T \approx T_P + g_0 T_N$. Then, $dT/dt \approx \rho T - \gamma T$ and the approximating solution is $T = T_{\text{shr}} e^{(\rho-\gamma)t}$ with slope $\rho - \gamma$. Finally, if the tumor cells were not extinct, the tumor response phase starts during the persistence phase of CAR-T cells with small number of effector CAR-T cells. Therefore, $dT/dt \approx \rho T$ and the approximating solution is $T = T_{\text{min}} e^{\rho t}$ with slope ρ.

Estimating model parameters from response characteristics

Our correlation analysis revealed that estimates of the slopes during the different response phases for CAR-T cells and tumor burden can be used to approximate 7 corresponding model parameters (Fig 3). We furthermore showed that 3 additional model parameters can be obtained from estimating minima/maxima of the response curve, thereby allowing to obtain initial estimates for 10 out of the 12 parameters for the fundamental model layer (equations (1-5), parameters μ_I, μ_E, μ_M, κ, η, ϵ, θ, ρ, γ A, B, K). In particular, the slopes observed in the CAR-T time courses determine μ_I (distribution slope), μ_E (contraction slope), μ_M (persistence slope) and κ (expansion slope summed wit μ_E), while the duration of the distribution phase determines η. The CAR-T cell peak height and time depend on a intricate relationship of A and B, while the persistence level determines ϵ. The slopes of the transient, shrinkage and response phases of tumor dynamics determine ρ and γ. The remaining parameter are the carrying capacity of tumor cells K, which can be estimated from literature and has no major effect on model dynamics, and the memory recruitment rate θ, which can be assessed by an approximation of the proportion of memory and effector CAR-T cells during the persistence phase. Using an iterative process that qualitatively fits the model solutions to the available time course data, we obtain initial estimates that can be further improved by an appropriate optimization algorithm (see below).

Assessing different sources of macrophage activation

To asses the different sources of macrophage activation, we split the macrophage population in three sub-populations according to the activation mechanism, $M_a = M_{a,K} + M_{a,B} + M_{a,C}$, where $M_{a,K}$ are the DAMP-activated macrophages, $M_{a,B}$ are the antigen-binding-activated macrophages and $M_{a,C}$ are the CD40-activated macrophages. The differential equations for each population are obtained by splitting

the activation rate (11), leading to

$$\frac{dM_{a,j}}{dt} = h_j M_i - \delta_M M_{a,j}, \quad j = K, B, C, \tag{12}$$

where the activation of each sub-population is given by

$$h_B = \beta_B \frac{T_P}{A + T_P} C_E, \quad h_K = \beta_K \frac{C_E}{B + C_E}(T_P + g_0 T_N), \quad h_C = \beta_C \frac{M_a}{C + M_a} C_E. \tag{13}$$

With this, we calculated for the simulated solutions the peak time for each macrophage population. Further, the total number of macrophages activated by each mechanism is obtained by evaluating the integrals $\int_0^{t_F} h_j M_i dt$, $j = K, B, C$ until a final time t_F.

Clinical data

Individual pharmacokinetic profiles of patients undergoing anti-CD19 CAR-T cell therapy were digitized from [1, 27, 36, 37], and we collected the raw data disclosed in [38]. A detection limit was set for CAR-T at 25 copies/μg DNA [38] or 2.5x10^5 cells (for conversions see Model setup and parameter fitting) and relapse was defined as the absolute number of total tumor cells exceeding its initial tumor burden.

We incorporated data from [1] for two pediatric patients. Patient 1 received a total of 1.2×10^7/kg CAR-T cells administered over three consecutive days, while Patient 2 received a single infusion of 1.4×10^6/kg CAR-T cells. Although specific initial tumor burden data were not provided, CD19 expression analysis in bone marrow samples of Patient 2 revealed a pre-treatment blast population comprising approximately 7.7% CD19- cells and 92.3% CD19+ cells. In the absence of peripheral blood measurements, we assumed the same distribution of antigen-negative and positive cells to set the initial tumor burden. Patient 2 experienced a clinical relapse evident in the peripheral blood two months post-infusion, while Patient 1 achieved clinical remission that persisted for nine months.

The dataset from [27] includes a phase I study with pediatric B-ALL patients treated using a second-generation CAR with a 4-1BB intracellular co-stimulatory domain. Each patient received one CAR-T cell infusion, with initial tumor burden estimated from pre-therapy peripheral blood blast percentages. Progression-free survival (PFS) days was used as relapse times. The IL-6-profile was represented as a heatmap for the first month, and we computed the average value to capture the time series results of IL-6 concentrations in serum.

We used data from [36], patients 1, 2, 3, and 4 diagnosed with ALL received treatment using autologous CAR with CD28 intracellular co-stimulatory domain, while patients 6 and 7 were treated with autologous CAR featuring CD137 intracellular co-stimulatory domain. The time-profile of CD19+ cells in lymphocytes in the blood, measured by flow cytometry, revealed that within 2-8 months, patients experienced either progression or relapse of CD19+ leukemia cells.

Finally, we used data from [38], for adult CLL patients treated with split-dose of autologous T-cells transduced with a CD19-directed CAR. With the exception of patient 22, who transformed to CD19-dim DLBCL, patients exhibited either complete or partial responses. For patients P01, P02 and P03, the initial CLL tumor burden and cytokine information (baseline and fold change) were extracted from [37] (respectively named UPN01, UPN03 and UPN02). Initial tumor burden on day -1 was available for UPN02 (P03), while for UPN01 (P01) and UPN03 (P02), only bone marrow data was provided, we assumed a similar approximation in blood due to its reasonable range.

An overview of patient and product characteristics and the corresponding infused doses and regimens are presented in Supplementary Table 2.

Model setup and parameter fitting

We encoded the model structure in QSP Designer [46] and employed Nelder-Mead method for parameter estimation, minimizing the weighted least squared error (WLS) between model simulations and data. The model was fitted separately to antigen-positive tumor cells and CAR-T cells, further adding antigen-negative tumor cells and IL-6. We applied zero-limits to CAR-T and tumor cell populations to limit artificial regrowth. That is, if any cell population reached less than 1 cell, proliferation was set to 0.

In instances where the initial tumor burden was either unspecified (NA) or had 0% blasts, we established a baseline of $T_P(0) = 10^7$ cells. Data points where %blasts were approximately 0 after therapy were not included in calibration due to the high uncertainty associated with digitization. For patients in the studies by Ma et al. [27] and Li et al. [36], where tumor burdens were expressed as percentages, we made an approximation based on the assumption that this percentages are related to white blood cells (WBC) and an adult has 5L of blood. Using an WBC range of $(2.0 - 6.5) \times 10^{10}$ provided in [47], we have an average of 4.25×10^{10} of WBC cells. The absolute number of tumor cells was then estimated using the formula: tumor cells = WBC cells × % blasts.

The administered dose of CAR-T cells represents the initial condition of the injected CAR-T cell population ($C_I(0)$). Initial populations of other phenotypes were set to zero since phenotypic differentiations occur throughout the dynamics' evolution ($C_E(0) = C_M(0) = 0$). For antigen-negative tumor cells, except for patient G02, the initial tumor burden ($T_N(0)$) was fitted below the detection limit of 2.5$\times 10^5$ cells. Inactive macrophages ($M_i(0)$) were fitted between 1-5$\times 10^9$ cells [48, 49], while active macrophages were set to zero ($M_a(0) = 0$).

The scaling factor for CAR-T cell count data was estimated using data provided by Lee et al. [50] and Kalos et al. [37], where both counts per microgram and total circulating cells were reported. The conversion factor was determined to be 1 CAR-T cell copy/μg DNA = 10^4 CAR-T cells. For conversions between the absolute number of CAR-T cells and cells/μL, we used the same blood volume of 5L in humans, which gives us 1 CAR-T cell/μL = 5×10^6 CAR-T cells. Furthermore, considering that about 1% of cells are present in the peripheral blood (PB) at all times compared to the bone marrow (BM), we have 1 CAR-T cell/μL in BM = 5×10^8 CAR-T cells in PB.

Data availability

The patient data that support the findings of this study were collected from existing literature [1, 27, 36, 37, 38] and are available from the corresponding author upon reasonable request.

References

[1] Stephan A Grupp, Michael Kalos, David Barrett, Richard Aplenc, David L Porter, Susan R Rheingold, David T Teachey, Anne Chew, Bernd Hauck, J Fraser Wright, et al. Chimeric antigen receptor–modified t cells for acute lymphoid leukemia. New England Journal of Medicine, 368 (16):1509–1518, 2013.

[2] Couto S. C. F. da Silva Santurio D. Paixão E. A. Cardoso-F. da Silva V. J. Klinger-P. Ribeiro P. D. A. C. Rós F. A. Oliveira T. G. M. Rego E. M. Ramos R. N. Rocha V. Barros, L. R. C. Systematic review of available car-t cell trials around the world. Cancers, 14(11):2667, 2022. doi: https://doi.org/10.3390/cancers14112667.

[3] Andrew M Stein, Stephan A Grupp, John E Levine, Theodore W Laetsch, Michael A Pulsipher, Michael W Boyer, Keith J August, Bruce L Levine, Lori Tomassian, Sweta Shah, et al. Tis-

agenlecleucel model-based cellular kinetic analysis of chimeric antigen receptor–t cells. CPT: pharmacometrics & systems pharmacology, 8(5):285–295, 2019.

[4] Can Liu, Vivaswath S Ayyar, Xirong Zheng, Wenbo Chen, Songmao Zheng, Hardik Mody, Weirong Wang, Donald Heald, Aman P Singh, and Yanguang Cao. Model-based cellular kinetic analysis of chimeric antigen receptor-t cells in humans. Clinical Pharmacology & Therapeutics, 109(3): 716–727, 2021.

[5] Emanuelle A Paixão, Luciana RC Barros, Artur C Fassoni, and Regina C Almeida. Modeling patient-specific car-t cell dynamics: Multiphasic kinetics via phenotypic differentiation. Cancers, 14(22):5576, 2022.

[6] Nirali N Shah and Terry J Fry. Mechanisms of resistance to car t cell therapy. Nature reviews Clinical oncology, 16(6):372–385, 2019.

[7] Daniela Silva Santurio, Emanuelle A Paixão, Luciana RC Barros, Regina C Almeida, and Artur C Fassoni. Mechanisms of resistance to car-t cell immunotherapy: Insights from a mathematical model. Applied Mathematical Modelling, 125:1–15, 2024.

[8] Theodoros Giavridis Michel Sadelain Emma C. Morris, Sattva S. Neelapu. Cytokine release syndrome and associated neurotoxicity in cancer immunotherapy. Nature Reviews Immunology, 22: 85–96, 2022. doi: 10.1038/s41577-021-00547-6.

[9] Partow Kebriaei William Wierda Cristina Gutierrez Frederick L. Locke Krishna V. Komanduri Yi Lin Nitin Jain Naval Daver Jason Westin Alison M. Gulbis Monica E. Loghin John F. de Groot Sherry Adkins Suzanne E. Davis Katayoun Rezvani Patrick Hwu Elizabeth J. Shpall Sattva S. Neelapu, Sudhakar Tummala. Chimeric antigen receptor t-cell therapy — assessment and management of toxicities. Nature Reviews Clinical Oncology, 18:47–62, 2018. doi: 10.1038/nrclinonc.2017.148.

[10] Anand Rotte, Matthew J Frigault, Ayub Ansari, Brad Gliner, Christopher Heery, and Bijal Shah. Dose–response correlation for car-t cells: a systematic review of clinical studies. Journal for ImmunoTherapy of Cancer, 10(12), 2022.

[11] Zhao L. Wang J. Yao Y. Wang J. Ji S. Hua T. Wang S. Cheng H. Shi M. Li Z. Zeng L. Zheng J. Xu K. Cao J. Wang, X. Correlation of cytokine release syndrome with prognosis after chimeric antigen receptor t cell therapy: Analysis of 54 patients with relapsed or refractory multiple myeloma. Frontiers in immunology, 13:814548, 2022. doi: https://doi.org/10.3389/fimmu.2022.814548.

[12] David T.; Grupp Stephan A. Barrett, David M.; Teachey. Toxicity management for patients receiving novel t-cell engaging therapies. Current Opinion in Pediatrics, 26:43–49, 2014. doi: 10.1097/MOP.0000000000000043.

[13] Gill S. Hexner E. O. Schuster S. Nasta S. Loren A. Svoboda J. Stadtmauer E. Landsburg D. J. Mato A. Levine B. L. Lacey S. F. Melenhorst J. J. Veloso E. Gaymon A. Pequignot E. Shan X. Hwang W. T. June C. H. Porter D. L. Frey, N. V. Long-term outcomes from a randomized dose optimization study of chimeric antigen receptor modified t cells in relapsed chronic lymphocytic leukemia. Journal of Clinical Oncology, 35:2862–2871, 2020. doi: 10.1200/JCO.19.03237.

[14] Eyquem J Hamieh M Piersigilli A Sadelain M. Giavridis T, van der Stegen SJC. Car t cell-induced cytokine release syndrome is mediated by macrophages and abated by il-1 blockade. Nature Medicine, 24(6):731–738, 2018. doi: doi:10.1038/s41591-018-0041-7.

[15] Theodoros Giavridis, Sjoukje JC van der Stegen, Justin Eyquem, Mohamad Hamieh, Alessandra Piersigilli, and Michel Sadelain. Car t cell–induced cytokine release syndrome is mediated by macrophages and abated by il-1 blockade. Nature medicine, 24(6):731–738, 2018.

[16] Margherita Norelli, Barbara Camisa, Giulia Barbiera, Laura Falcone, Ayurzana Purevdorj, Marco Genua, Francesca Sanvito, Maurilio Ponzoni, Claudio Doglioni, Patrizia Cristofori, et al. Monocyte-derived il-1 and il-6 are differentially required for cytokine-release syndrome and neurotoxicity due to car t cells. Nature medicine, 24(6):739–748, 2018.

[17] M. Rosa V. M. Pérez-García S. Chulián, Á. Martínez-Rubio. Mathematical models of leukaemia and its treatment: a review. SeMA, 79:487–488, 2022. doi: https://doi.org/10.1007/s40324-022-00305-1.

[18] Altrock PM Kimmel GJ, Locke FL. The roles of t cell competition and stochastic extinction events in chimeric antigen receptor t cell therapy. Proceedings. Biological sciences, 288:1947, 2021. doi: https://doi.org/10.1098/rspb.2021.0229.

[19] Cristina Blázquez Goñi Manuel Ramírez Orellana Antonio Pérez Martínez Alfonso Navarro-Zapata Cristina Ferreras Victor M Pérez-García María Rosa Álvaro Martínez-Rubio, Salvador Chulián. A mathematical description of the bone marrow dynamics during car t-cell therapy in b-cell childhood acute lymphoblastic leukemia. International journal of molecular sciences, 22:6371, 2021.

[20] Xella A. Woodall R. Adhikarla V. Cho H. Gutova M. Brown C. E.- Rockne R. C. Brummer, A. B. Data driven model discovery and interpretation for car t-cell killing using sparse identification and latent variables. Frontiers in immunology, 2023. doi: https://doi.org/10.3389/fimmu.23.1115536.

[21] Reihaneh Mostolizadeh, Zahra Afsharnezhad, and Anna Marciniak-Czochra. Mathematical model of chimeric anti-gene receptor (car) t cell therapy with presence of cytokine. Numerical Algebra, Control and Optimization, 8(1):63–80, 2018. ISSN 2155-3289. doi: 10.3934/naco.2018004. URL https://www.aimsciences.org/article/id/cdf9226a-bcca-4de3-8c0b-bbccf912314b.

[22] Odelaisy León-Triana, Soukaina Sabir, Gabriel F. Calvo, Juan Belmonte-Beitia, Salvador Chulián, Álvaro Martínez-Rubio, María Rosa, Antonio Pérez-Martínez, Manuel Ramirez-Orellana, and Víctor M. Pérez-García. Car t cell therapy in b-cell acute lymphoblastic leukaemia: Insights from mathematical models. Communications in Nonlinear Science and Numerical Simulation, 94:105570, 2021. ISSN 1007-5704. doi: https://doi.org/10.1016/j.cnsns.2020.105570. URL https://www.sciencedirect.com/science/article/pii/S1007570420304007.

[23] Deni Hardiansyah and Chee Meng Ng. Quantitative systems pharmacology model of chimeric antigen receptor t-cell therapy. Clinical and translational science, 12(4):343–349, 2019.

[24] Reihaneh Mostolizadeh, Zahra Afsharnezhad, and Anna Marciniak-Czochra. Mathematical model of chimeric anti-gene receptor (car) t cell therapy with presence of cytokine. Numer. Algebr. Control Optim, 8(1):63–80, 2018.

[25] Zhuoyu Zhang, Lunan Liu, Chao Ma, and Weiqiang Chen. A computational model of cytokine release syndrome during car t-cell therapy. Advanced therapeutics, 5(10):2200130, 2022.

[26] Rob J De Boer and Alan S Perelson. Quantifying t lymphocyte turnover. Journal of theoretical biology, 327:45–87, 2013.

[27] Futian Ma, Jin-Yuan Ho, Huan Du, Fan Xuan, Xiaoli Wu, Qinglong Wang, Lin Wang, Ying Liu, Min Ba, Yizhuo Wang, et al. Evidence of long-lasting anti-cd19 activity of engrafted cd19 chimeric antigen receptor–modified t cells in a phase i study targeting pediatrics with acute lymphoblastic leukemia. Hematological oncology, 37(5):601–608, 2019.

[28] Mohamed-Reda Benmebarek, Clara Helke Karches, Bruno Loureiro Cadilha, Stefanie Lesch, Stefan Endres, and Sebastian Kobold. Killing mechanisms of chimeric antigen receptor (car) t cells. International journal of molecular sciences, 20(6):1283, 2019.

[29] Sophia Faude, Jane Wei, Kavitha Muralidharan, Xiaoming Xu, Gerald Wertheim, Michele Paessler, Vijay G Bhoj, Stephan A Grupp, Shannon L Maude, Susan R Rheingold, et al. Absolute lymphocyte count proliferation kinetics after car t-cell infusion impact response and relapse. Blood advances, 5(8):2128–2136, 2021.

[30] Zhen Jin, Rufang Xiang, Kai Qing, Xiaoyang Li, Yunxiang Zhang, Lining Wang, Hongming Zhu, Yuanfei Mao, Zizhen Xu, and Junmin Li. The severe cytokine release syndrome in phase i trials of cd19-car-t cell therapy: a systematic review. Annals of hematology, 97:1327–1335, 2018.

[31] Jianshu Wei, Yang Liu, Chunmeng Wang, Yajing Zhang, Chuan Tong, Guanghai Dai, Wei Wang, John EJ Rasko, J Joseph Melenhorst, Wenbin Qian, et al. The model of cytokine release syndrome in car t-cell treatment for b-cell non-hodgkin lymphoma. Signal Transduction and Targeted Therapy, 5(1):134, 2020.

[32] Ala Dibas, Manuel Rhiel, Vidisha Bhavesh Patel, Geoffroy Andrieux, Melanie Boerries, Tatjana I Cornu, Jamal Alzubi, and Toni Cathomen. Cell-based models of 'cytokine release syndrome'endorse cd40l and granulocyte–macrophage colony-stimulating factor knockout in chimeric antigen receptor t cells as mitigation strategy. Cells, 12(21):2581, 2023.

[33] Valerie Wittibschlager, Ulrike Bacher, Katja Seipel, Naomi Porret, Gertrud Wiedemann, Claudia Haslebacher, Michèle Hoffmann, Michael Daskalakis, Dilara Akhoundova, and Thomas Pabst. Car t-cell persistence correlates with improved outcome in patients with b-cell lymphoma. International journal of molecular sciences, 24(6):5688, 2023.

[34] Mattia Novo, M Hasib Sidiqi, Jonas Paludo, Sangeetha Gandhi, Jilan Kubusek, Tuan Truong, Justin Hayne, Stephen M Ansell, N Nora Bennani, Jose C Villasboas, et al. Peak lymphocyte count after car t infusion is a clinically accessible test that correlates with clinical response in axicabtagene ciloleucel therapy for lymphoma. Blood, 134:4106, 2019.

[35] Jie Li, Zhenyu Wu, and Naiqing Zhao. Individual patient data meta-analysis from 16 trials for safety factors in cytokine release syndrome after car-t therapy in patients with non-hodgkin lymphoma (nhl) and acute lymphoblastic leukemia. Advances in therapy, 36:2881–2894, 2019.

[36] Shiqi Li, Jiasi Zhang, Meiling Wang, Gang Fu, Yunyan Li, LI Pei, Zhouxing Xiong, Dabing Qin, Rui Zhang, Xiaobo Tian, et al. Treatment of acute lymphoblastic leukaemia with the second generation of CD 19 CAR-T containing either CD28 or 4-1BB. British Journal of Haematology, 181(3):360–371, 2018. doi: 10.1111/bjh.15195.

[37] Michael Kalos, Bruce L Levine, David L Porter, Sharyn Katz, Stephan A Grupp, Adam Bagg, and Carl H June. T cells with chimeric antigen receptors have potent antitumor effects and can establish memory in patients with advanced leukemia. Science translational medicine, 3(95):95ra73–95ra73, 2011.

[38] David L Porter, Wei-Ting Hwang, Noelle V Frey, Simon F Lacey, Pamela A Shaw, Alison W Loren, Adam Bagg, Katherine T Marcucci, Angela Shen, Vanessa Gonzalez, et al. Chimeric antigen receptor t cells persist and induce sustained remissions in relapsed refractory chronic lymphocytic leukemia. Science translational medicine, 7(303):303ra139–303ra139, 2015.

[39] Stephen J Schuster, Richard T Maziarz, Elisha S Rusch, Junlong Li, James E Signorovitch, Vadim V Romanov, Frederick L Locke, and David G Maloney. Grading and management of cytokine release syndrome in patients treated with tisagenlecleucel in the juliet trial. Blood Advances, 4(7):1432–1439, 2020.

[40] Daniel W Lee, Bianca D Santomasso, Frederick L Locke, Armin Ghobadi, Cameron J Turtle, Jennifer N Brudno, Marcela V Maus, Jae H Park, Elena Mead, Steven Pavletic, et al. Astct consensus grading for cytokine release syndrome and neurologic toxicity associated with immune effector cells. Biology of blood and marrow transplantation, 25(4):625–638, 2019.

[41] David Porter, Noelle Frey, Patricia A Wood, Yanqiu Weng, and Stephan A Grupp. Grading of cytokine release syndrome associated with the car t cell therapy tisagenlecleucel. Journal of hematology & oncology, 11:1–12, 2018.

[42] Daniel W Lee, Rebecca Gardner, David L Porter, Chrystal U Louis, Nabil Ahmed, Michael Jensen, Stephan A Grupp, and Crystal L Mackall. Current concepts in the diagnosis and management of cytokine release syndrome. Blood, The Journal of the American Society of Hematology, 124(2): 188–195, 2014.

[43] Daniel C Kirouac, Cole Zmurchok, Avisek Deyati, Jordan Sicherman, Chris Bond, and Peter W Zandstra. Deconvolution of clinical variance in car-t cell pharmacology and response. Nature biotechnology, pages 1–12, 2023.

[44] Lunan Liu, Chao Ma, Zhuoyu Zhang, Matthew T Witkowski, Iannis Aifantis, Saba Ghassemi, and Weiqiang Chen. Computational model of car t-cell immunotherapy dissects and predicts leukemia patient responses at remission, resistance, and relapse. Journal for ImmunoTherapy of Cancer, 10(12), 2022.

[45] Emma C Morris, Sattva S Neelapu, Theodoros Giavridis, and Michel Sadelain. Cytokine release syndrome and associated neurotoxicity in cancer immunotherapy. Nature Reviews Immunology, 22(2):85–96, 2022.

[46] Richard J Matthews, David Hollinshead, Daniel Morrison, Piet H van Der Graaf, and Andrzej M Kierzek. Qsp designer: Quantitative systems pharmacology modeling with modular biological process map notation and multiple language code generation. CPT: Pharmacometrics & Systems Pharmacology, 2023.

[47] JM Pekelharing, O Hauss, R De Jonge, J Lokhoff, J Sodikromo, M Spaans, Rob Brouwer, S De Lathouder, and R Hinzmann. Haematology reference intervals for established and novel parameters in healthy adults. Sysmex Journal International, 20(1):1–9, 2010.

[48] Ron Sender, Yarden Weiss, Yoav Navon, Idan Milo, Nofar Azulay, Leeat Keren, Shai Fuchs, Danny Ben-Zvi, Elad Noor, and Ron Milo. The total mass, number, and distribution of immune cells in the human body. Proceedings of the National Academy of Sciences, 120(44):e2308511120, 2023.

[49] Dorothy Hudig, Kenneth W Hunter, W John Diamond, and Doug Redelman. Properties of human blood monocytes. ii. monocytes from healthy adults are highly heterogeneous within and among individuals. Cytometry Part B: Clinical Cytometry, 86(2):121–134, 2014.

[50] Daniel W Lee, James N Kochenderfer, Maryalice Stetler-Stevenson, Yongzhi K Cui, Cindy Delbrook, Steven A Feldman, Terry J Fry, Rimas Orentas, Marianna Sabatino, Nirali N Shah, et al. T cells expressing cd19 chimeric antigen receptors for acute lymphoblastic leukaemia in children and young adults: a phase 1 dose-escalation trial. The Lancet, 385(9967):517–528, 2015.

Acknowledgements

ACF was supported by Alexander von Humboldt Foundation and Coordenação de Aperfeiçoamento de Pessoal de Nível Superior - Brasil (CAPES).

Author contributions

Conceptualization: DSS, LRCB, IG, ACF. Formal Analysis, investigation, methodology: DSS, ACF. Writing: DSS, LRCB, IG, ACF. Supervision: ACF.

Competing interests

The authors declare that they have no conflict of interest.

Mathematical modeling unveils the timeline of CAR-T cell therapy and macrophage-mediated cytokine release syndrome

Supplementary Information

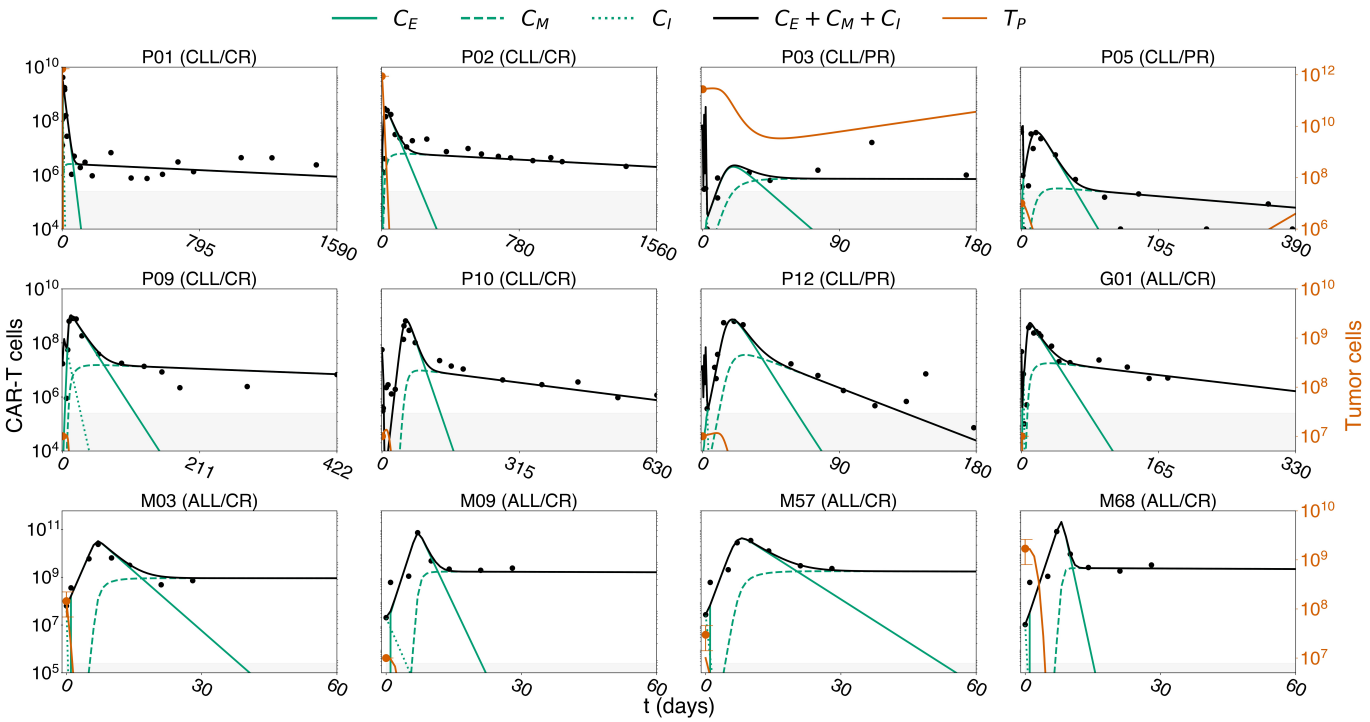

Supplementary Figure 1. Model simulations for responders. Model fits for selected patients that showed either complete response (CR) or partial response (PR). CR is achieved when the tumor is clinically undetectable, while PR is defined by a final tumor burden at least less than 50% of the initial burden. The CAR-T cell detection threshold of 2.5×10^5 cells is represented by the gray shaded area.

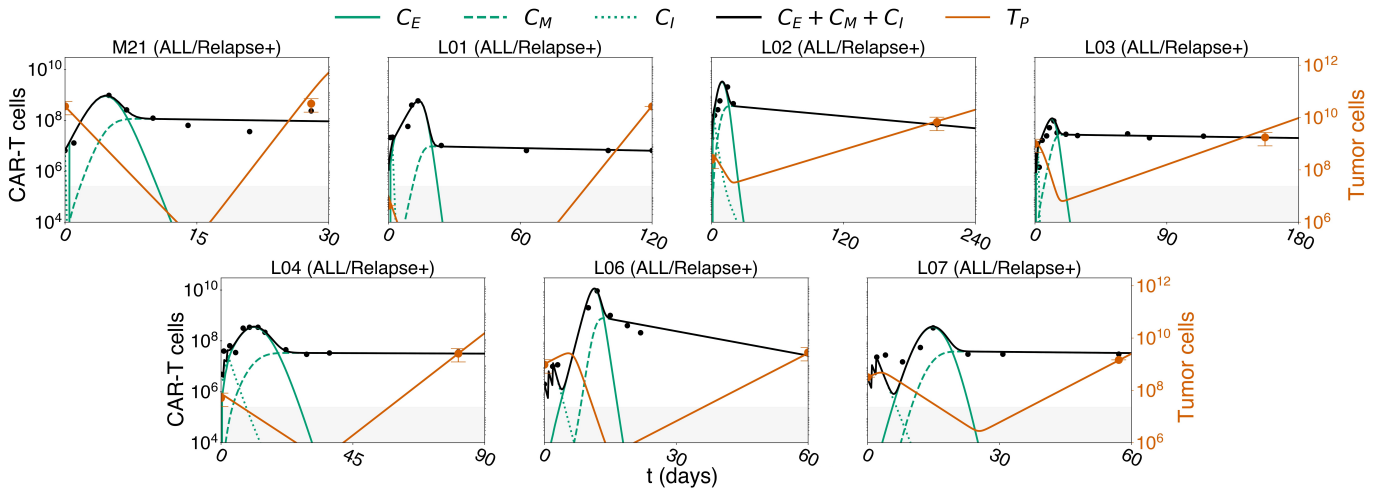

Supplementary Figure 2. Model simulations for patients with antigen-positive relapse. Model fits for selected patients, excluding data points where %blasts approached zero. Tumor cell error bars represent the range of WBCs used in scaling (see Methods). The CAR-T cell detection threshold of 2.5×10^5 cells is represented by the gray shaded area.

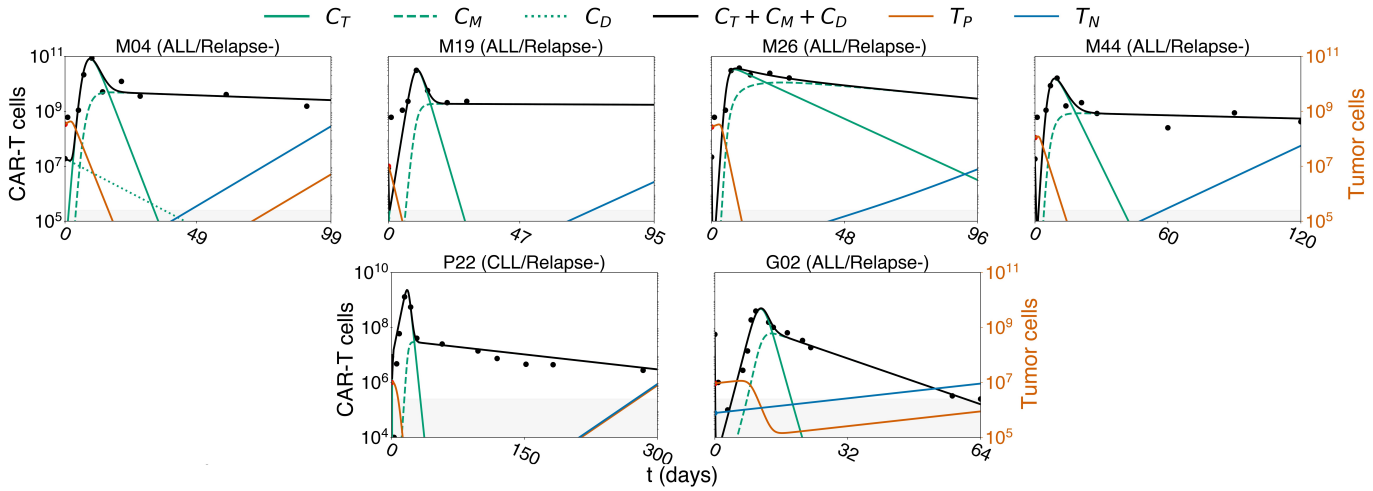

Supplementary Figure 3. Model simulations for patients with antigen-negative relapse. Model fits for selected patients, antigen-negative tumor cells, except for patient G02, the initial tumor burden ($T_N(0)$) was fitted below the detection limit of 2.5$\times 10^5$ cells (gray shaded area).

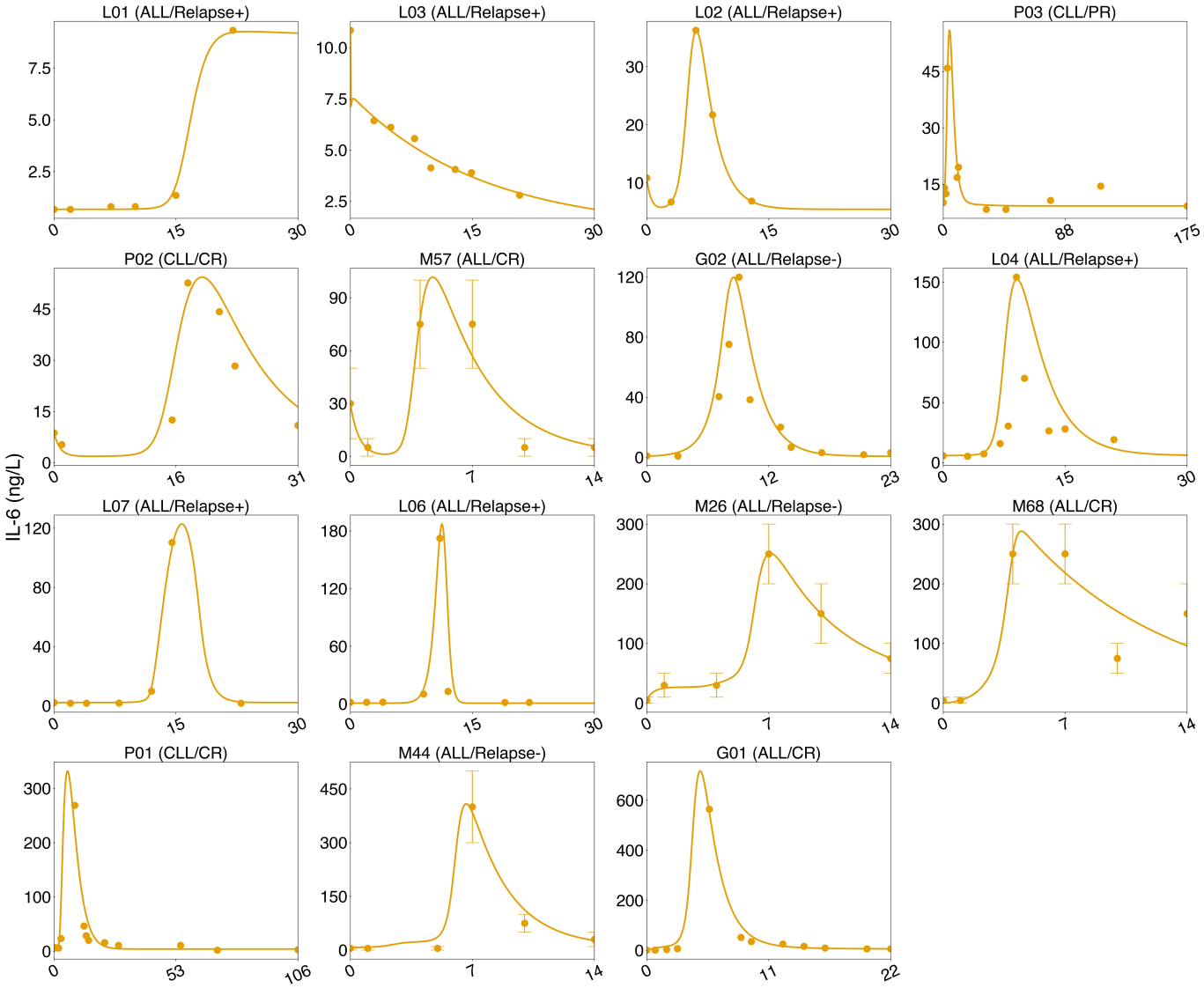

Supplementary Figure 4. Model simulations of IL-6 kinetics for selected patients. Experimental data points (orange dots) from [1, 38, 36, 27] are compared with model predictions (orange line). When data was presented data as serum fold change, we establish a direct relationship by considering either a baseline value of 1 ng/L [1] or the specific baseline values provided for each patient [37, 38]. The mean values within the reported range for dataset [27] are visually represented by bars in the figure.

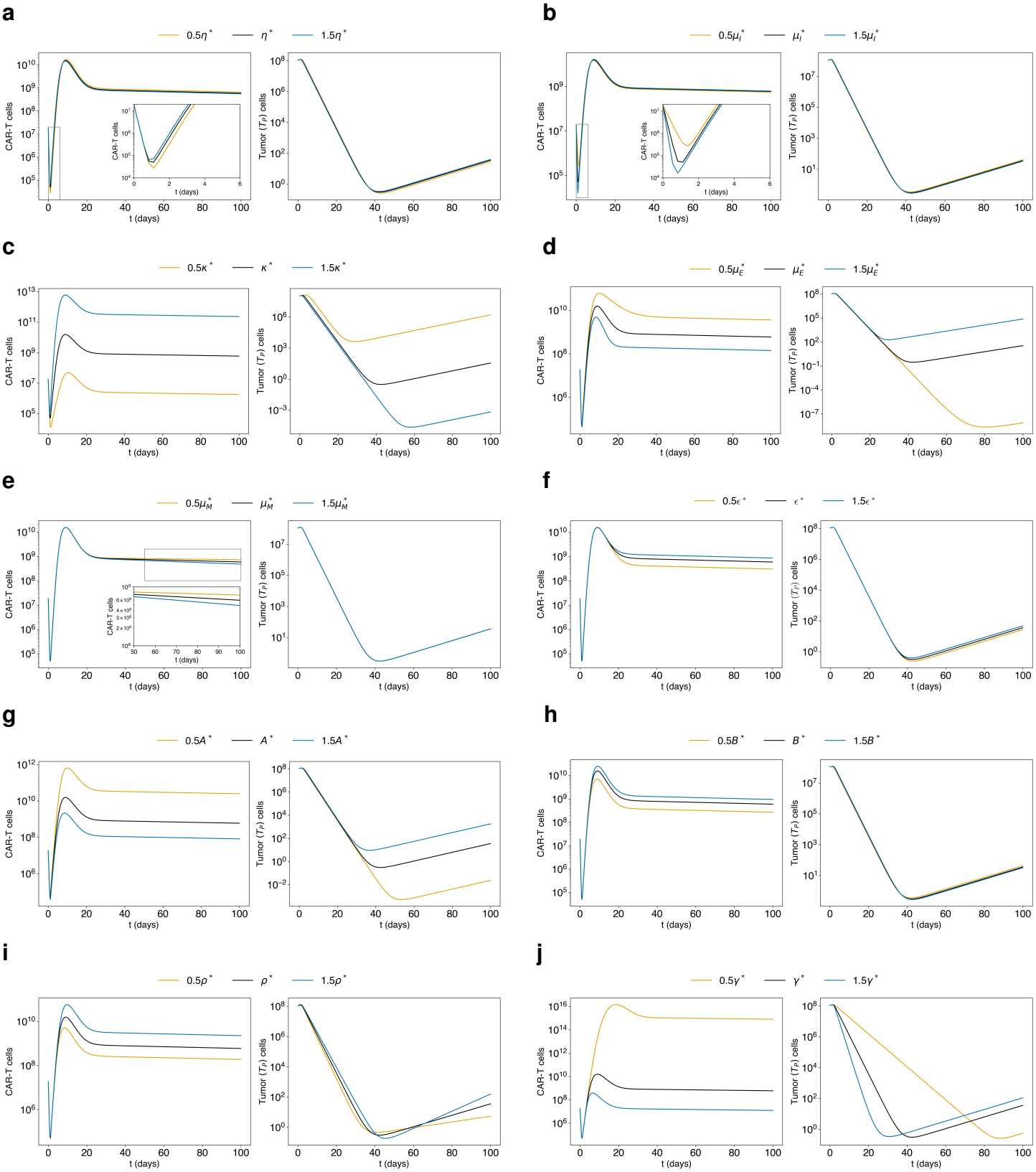

Supplementary Figure 5. Qualitative sensitivity analysis. Model simulations for patient M44, changing one parameter at time, where * represents the fitted value.

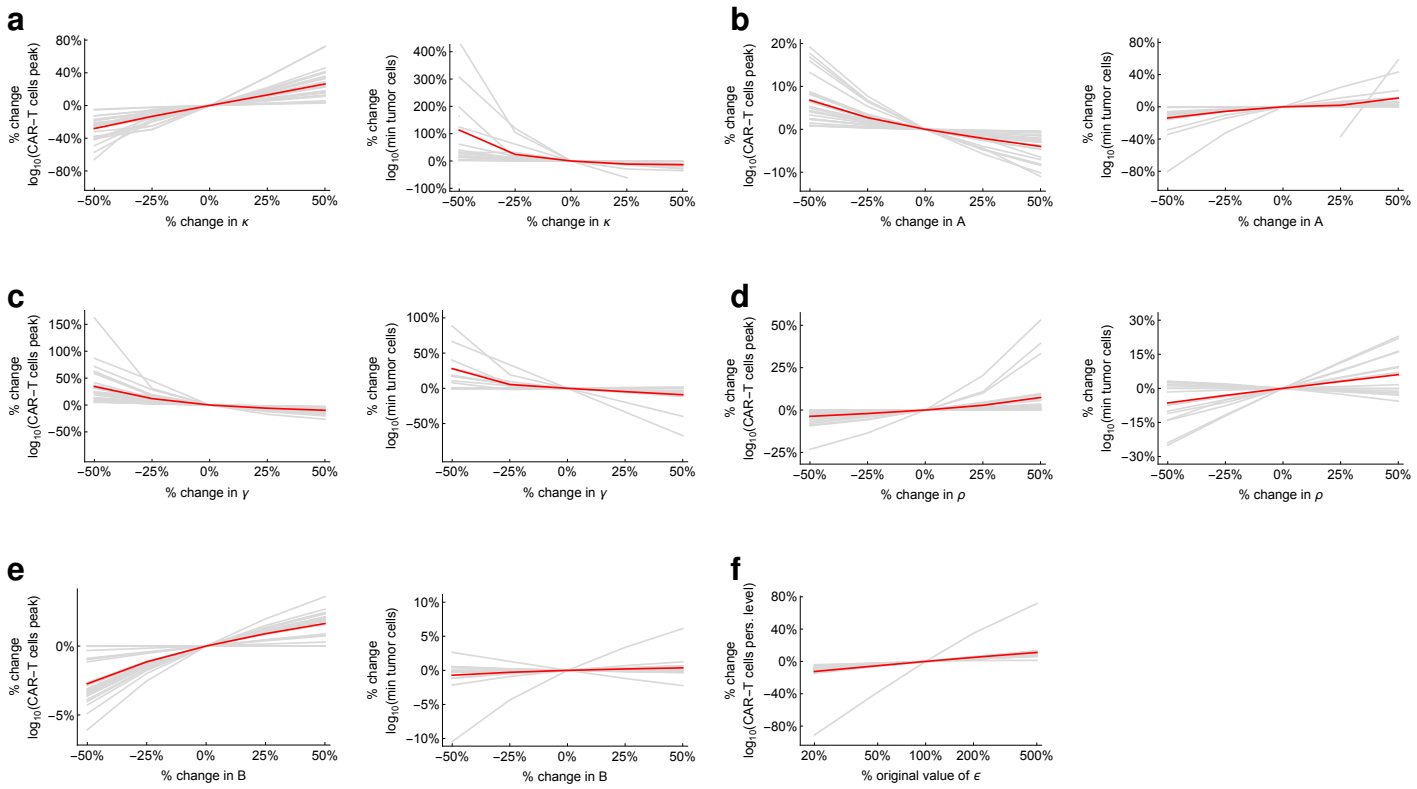

Supplementary Figure 6. Sensitivity analysis. Effects of parameter changes on the numbers of CAR-T cells at peak, minimum tumor load reached during shrinkage phase (a-e) and CAR-T cell persistence (f), measured by the number of CAR-T cells at day 150 after infusion. Gray lines show the effect for the 25 individual patients while the red line shows the mean.

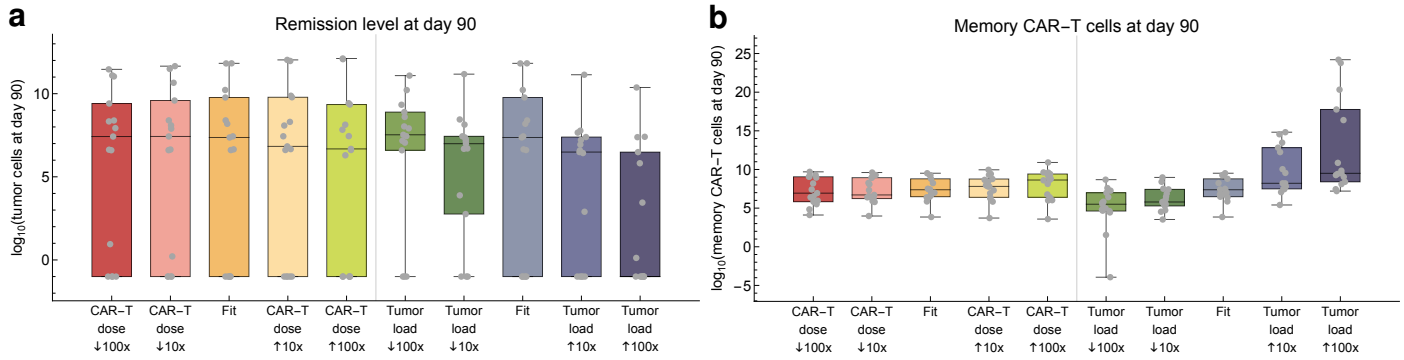

Supplementary Figure 7. Effect of different dosing protocols on CAR-T cell dynamics and tumor response. Comparing the standard scenario (Fit) with simulations starting with either a different CAR-T dose or initial tumor burden (10x and 100x smaller and higher). Assessed outcomes: **a** number of tumor cells at day 90, **b** number of memory CAR-T cells at day 90.

Supplementary Table 1: Model parameters and functions with their units and biological meaning.

Parameter	Unit	Biological meaning
μ_I	day^{-1}	Death rate of injected CAR-T cells
η	day^{-1}	Engraftment rate of injected cells to blood and tumor niche
κ	day^{-1}	Expansion rate of effector CAR-T cells
A	cell	Half-saturation constant for antigen-receptor binding functional response
μ_E	day^{-1}	Reduction rate (apoptosis and exhaustion) of effector CAR-T cells
ϵ	day^{-1}	Rate of memory formation
θ	day^{-1}	Rate of memory recruitment
μ_M	day^{-1}	Death rate of memory CAR-T cells
ρ	day^{-1}	Proliferation rate of tumor cells
K	cell	Carrying capacity of tumor cells
γ	day^{-1}	Kill rate of effector CAR-T cells on antigen-positive tumor cells
g_0	1	Reduction factor for the kill rate of effector CAR-T cells on antigen-negative tumor cells
B	cell	Half-saturation constant for tumor kill functional response
σ_M	(ng/L)day^{-1}	Basal production of naive macrophages
δ_M	day^{-1}	Macrophages death rate
β_K	(day.cell)$^{-1}$	Macrophage activation rate due to DAMP release
β_B	(day.cell)$^{-1}$	Macrophage activation rate due to antigen-binding
β_C	(day.cell)$^{-1}$	Macrophage activation rate due to CD-40 contact
C	cell	Half-saturation constant for macrophage activation rate due to CD-40 contact
σ_I	(ng/L)day^{-1}	Endogenous cytokine production
δ_I	day^{-1}	Cytokine natural decay rate
α	(ng/L)(day.cell)$^{-1}$	Cytokine production rate by macrophages

Supplementary Table 2: Individual CAR-T cell dose, the end of analysis, disease, outcome, initial tumor burden and baseline IL-6 concentration. In the split-dose regimen, the CAR-T cell dose was given in 3 fractions with 10% administered on day 0, 30% on day 1, and the remaining 60% on day 3).

Patient	Regimen	CAR-T dose ($\times 10^6$)	Weight (kg)	Product	End of analysis (days)	Outcome	Initial Tumor Burden	IL-6 (0) (ng/L)
Grupp et al., [1] - ALL								
G01	Split-dose	12 (cells/kg)	40*	CD28	330	CR	NA	1 †††
G02**	Single-dose	1.4 (cells/kg)	40*	CD28	64	$Relapse-$	7.7% (T_N) 92.3% (T_P)	1 †††
Porter et al., [38] - CLL								
P01	Split-dose	1130 (cells)	-	4-1BB	1590	CR	1.7×10^{12} (cells)	7
P02	Split-dose	14.2 (cells)	-	4-1BB	1560	CR	8.8×10^{11} (cells)	8.7
P03	Split-dose	586 (cells)	-	4-1BB	180	PR	2.75×10^{11} (cells)	10.1
P05	Split-dose	392 (cells)	-	4-1BB	390	PR	NA	-
P09	Split-dose	170.0 (cells)	-	4-1BB	422	CR	NA	-
P10	Split-dose	56.1 (cells)	-	4-1BB	630	CR	NA	-
P12	Split-dose	118.0 (cells)	-	4-1BB	180	PR	NA	-
P22	Split-dose	86.4 (cells)	-	4-1BB	300	PR	NA	-
Li et al., [36] - ALL								
L01	Split-dose	13.3 (cells)	-	CD28	120	$Relapse+$	0.0% ††	0.68 ††
L02	Split-dose	199.6 (cells)	-	CD28	240	$Relapse+$	0.57% ††	10.85 ††
L03	Split-dose	44.3 (cells)	-	CD28	180	$Relapse+$	2.28% ††	10.85 ††
L04	Split-dose	48.8 (cells)	-	CD28	90	$Relapse+$	0.12% ††	5.75 ††
L06	Split-dose	19.9 (cells)	-	CD137	60	$Relapse+$	2.28% ††	1.765 ††
L07	Split-dose	33 (cells)	-	CD137	60	$Relapse+$	0.65% ††	2.17 ††
Ma et al., [27] - B-ALL								
M03	Single-dose	1.58 (cells/kg)	40	4-1BB	734†	CR	0.34%	-
M04	Single-dose	0.73 (cells/kg)	26	4-1BB	99†	$Relapse-$	0.80%	-
M09	Single-dose	1.0 (cells/kg)	20.5	4-1BB	620†	CR	0%	-
M19	Single-dose	0.50 (cells/kg)	17	4-1BB	95†	$Relapse-$	0%	-
M21	Single-dose	0.30 (cells/kg)	22	4-1BB	30†	$Relapse+$	63%	-
M26	Single-dose	0.50 (cells/kg)	43	4-1BB	96†	$Relapse-$	0.63%	≤ 10
M44	Single-dose	0.50 (cells/kg)	37	4-1BB	120†	$Relapse-$	0.26%	≤ 10
M57	Single-dose	0.50 (cells/kg)	54	4-1BB	280†	CR	0.07%	10-50
M68	Single-dose	0.50 (cells/kg)	21	4-1BB	244†	CR	4%	≤ 10

* Estimated based on the patient's age.
** Percentage from total of tumor cells, which was not assessed.
† Estimated based on the progression-free survival day.
†† Estimated using WebPlotDigitizer
††† Cytokine concentrations were displayed as factor change from baseline, and for simplicity in fitting and conversion, we assumed IL-6(0)=1 ng/L
NA = Not assessed.